Multi-transcriptomic analysis points to early organelle dysfunction in human astrocytes in Alzheimer's disease

Running title: Astrocyte-targeted Alzheimer therapeutics

Elena Galea[1,2,3*], Laura D. Weinstock[4], Raquel Larramona-Arcas[1,2], Alyssa F. Pybus[4], Lydia Giménez-Llort[1,5], Carole Escartin[6], Levi B. Wood[4,7]

1. Institut de Neurociències, Universitat Autònoma de Barcelona, Bellaterra, 08193 Barcelona, Spain.
2. Departament de Bioquímica, Unitat de Bioquímica, Universitat Autònoma de Barcelona, 08193 Barcelona, Spain.
3. ICREA, 08010 Barcelona, Spain.
4. Wallace H. Coulter Department of Biomedical Engineering, Georgia Institute of Technology, Atlanta, 30332 USA.
5. Departament de Psiquiatria i Medicina Forense, Universitat Autònoma de Barcelona, Bellaterra, 08193 Barcelona, Spain.
6. Université Paris-Saclay, CEA, CNRS, MIRCen, Laboratoire des Maladies Neurodégénératives, 92265, Fontenay-aux-Roses, France.
7. George W. Woodruff School of Mechanical Engineering and Parker H. Petit Institute for Bioengineering and Bioscience, Georgia Institute of Technology, Atlanta, 30332 USA.

Corresponding authors:
levi.wood@me.gatech.edu; +1 (617) 388 9950
Elena.Galea@uab.es; +34 935 868 143.

Word count: 11663
1. Abstract: 250
2. Introduction: 796
3. Material and methods: 1779
4. Results: 3667
5. Discussion: 3078
6. Figure legends: 1259
7. Supplementary data legends: 834

Acknowledgements:

The authors thank Dr. Alberto Lleó of the Unitat de Memòria at the Hospital Sant Pau, Barcelona, Spain, for critical reading of the manuscript. This work was supported by Fundació Marato-TV3 (grant number 201414-30), and Grup de Recerca en demències: Sant Pau SGR2017547, Generalitat de Catalunya (E.G.), by funds from the Coins for Alzheimer's Research Trust (L.B.W.) and startup funds from the Woodruff School of Mechanical Engineering at Georgia Tech (L.B.W.). L.D.W. and A.F.P were supported in part by the National Institutes of Health Cell and Tissue Engineering Biotechnology Training Grant (T32-GM008433). CNRS, CEA and France Alzheimer (C.E.). The results published here are in whole or in part based on data obtained from the AD Knowledge Portal (https://adknowledgeportal.synapse.org). Study data were provided by the following sources: The Mayo Clinic Alzheimers Disease Genetic Studies, led by Dr. Nilufer Ertekin-Taner and Dr. Steven G. Younkin, Mayo Clinic, Jacksonville, FL using samples from the Mayo Clinic Study of Aging, the Mayo Clinic Alzheimers Disease Research Center, and the Mayo Clinic Brain Bank. Data collection was

supported through funding by NIA grants P50 AG016574, R01 AG032990, U01 AG046139, R01 AG018023, U01 AG006576, U01 AG006786, R01 AG025711, R01 AG017216, R01 AG003949, NINDS grant R01 NS080820, CurePSP Foundation, and support from Mayo Foundation. Study data includes samples collected through the Sun Health Research Institute Brain and Body Donation Program of Sun City, Arizona. The Brain and Body Donation Program is supported by the National Institute of Neurological Disorders and Stroke (U24 NS072026 National Brain and Tissue Resource for Parkinson's Disease and Related Disorders), the National Institute on Aging (P30 AG19610 Arizona Alzheimer's Disease Core Center), the Arizona Department of Health Services (contract 211002, Arizona Alzheimer's Research Center), the Arizona Biomedical Research Commission (contracts 4001, 0011, 05-901 and 1001 to the Arizona Parkinson's Disease Consortium) and the Michael J. Fox Foundation for Parkinson's Research. Study data were also provided by the Rush Alzheimer's Disease Center, Rush University Medical Center, Chicago. Data collection was supported through funding by NIA grants P30AG10161 (ROS), R01AG15819 (ROSMAP; genomics and RNAseq), R01AG17917 (MAP), R01AG30146, R01AG36042 (5hC methylation, ATACseq), RC2AG036547 (H3K9Ac), R01AG36836 (RNAseq), R01AG48015 (monocyte RNAseq) RF1AG57473 (single nucleus RNAseq), U01AG32984 (genomic and whole exome sequencing), U01AG46152 (ROSMAP AMP-AD, targeted proteomics), U01AG46161(TMT proteomics), U01AG61356 (whole genome sequencing, targeted proteomics, ROSMAP AMP-AD), the Illinois Department of Public Health (ROSMAP), and the Translational Genomics Research Institute (genomic). ROSMAP data can be requested at www.radc.rush.edu. All data generated during this study are included in this published article and its supplementary information files. Codes are available upon reasonable request.

Authors state no conflict of interest

Current address R. Larramona: Celltec-UB, Departament de Biologia Cel.lular, Fisiologia i Immunologia, Universitat de Barcelona, 08028; Institut de Neurociències, Universitat de Barcelona, 08035, Barcelona, Spain.

Abstract

Recent single-nucleus RNA sequencing of astrocytes in *postmortem* Alzheimer's disease (AD) samples is limited by the low number of sequenced astrocytes and small cohort sizes. We developed a systems biology approach to identify astrocytic genes in public large bulk AD transcriptomes. Brain cell specific gene clusters were generated from RNA sequencing data from isolated healthy human brain cells using cell-type enrichment scoring and clustering. Cell-specific gene clusters were localized in whole-brain transcriptomes from 766 subjects diagnosed with AD or mild cognitive impairment (MCI) from the Mount Sinai Hospital, the Mayo Clinic, and the Religious Order Study/Memory and Aging Project (ROSMAP). Gene clusters were organized into manually curated functional categories including astrocytic categories absent from existing platforms, such as perisynaptic astrocytic processes (PAP). Changes among subjects were determined by gene set variation analysis (GSVA) and principal component analysis (PCA). Hierarchical clustering revealed molecular heterogeneity in individuals with the same clinical diagnosis. Particularly in the Mayo Clinic and ROSMAP cohorts, over 50% of Controls presented the massive down-regulation of genes encoding synaptic proteins typical of AD, whereas 30% of AD patients presented Control-like transcriptomic profiles. According to GSVA and PCA, down-regulation of neuronal genes related to synaptic proteins correlated with down-regulation of astrocytic genes encoding mitochondrial and endolysosomal proteins, and up-regulation of genes related to PAP. Transcriptomic data thus unravel a deep phenotypic transformation of human astrocytes in AD, affecting organelles and astrocyte-neuron interactions. We posit that therapies preventing organelle dysfunction in astrocytes may protect neural circuits in preclinical and clinical AD.

Key words

Alzheimer's disease, astrocytes, hierarchical clustering, MCI, mitochondria, perisynaptic astrocyte processes, RNA seq.

124 **Main points**

125 1. Transcriptomes of control subjects and AD patients segregate in two main molecular profiles
126 regardless of clinical diagnosis.
127 2. Dysregulation of the endolysosomal/mitochondrial axis in astrocytes correlates with impaired
128 synaptic plasticity in neurons.
129
130

131

132 # Introduction

133 'Reactive' GFAP-overexpressing astrocytes are found in the vicinity of amyloid-β plaques in
134 *postmortem* brains from patients with Alzheimer's disease (AD), in both the autosomal-dominant
135 Alzheimer's disease (ADAD) and the sporadic late-onset (AD) variants, as well as in mouse models of
136 ADAD. The robust morphological transformation of astrocytes points to major phenotypical and,
137 hence, functional alterations in astrocytes in AD (reviewed in (Perez-Nievas & Serrano-Pozo, 2018)).

138 However, despite non-negligible research in the last decade, knowledge about phenotypical
139 alterations in human astrocytes from AD patients is still limited due, in part, to scarce and conflicting
140 human astrocyte-specific omics data. Prior studies include transcriptomics of laser-microdissected
141 astrocytes (Sekar et al., 2015; Simpson et al., 2011), co-expresion-based gene clustering of whole-brain
142 AD transcriptomes (B. Zhang et al., 2013) (Neff, 2021), and single-cell RNA sequencing (scRNAseq)
143 analyses (Grubman et al., 2019; Mathys et al., 2019).

144 Laser-microdissected astrocytes either presented insufficient number of differentially-expressed
145 genes (DEG) for pathway analysis (Sekar et al., 2015), or normalization anomalies, as suggested by
146 the finding that 98% of the DEGs were down-regulated (Simpson et al., 2011). The problem may lie in
147 the low RNA yields of laser microdissection, exacerbated by the poor RNA quality after long *post-*
148 *mortem* intervals. As an alternative to laser microdissection, clustering statistics based on gene co-
149 expression identified function-specific gene modules using whole-brain AD transcriptomes (B. Zhang
150 et al., 2013). Cellular localization of modules was established using cell-specific markers, and causality
151 between nodes was then inferred with Bayesian statistics. Using this approach, alterations of
152 glutamate and amino acid metabolism in an astrocytic module of 260 genes were discovered to be
153 well-ranked for causal relevance in AD, but no further changes were unraveled. Finally, although
154 scRNAseq and single-nucleus (sn)RNAseq improve the cellular resolution of transcriptomics to the
155 point of unraveling populations within a given cell-type, two challenges arise in studying astrocytes
156 with these techniques. One is the low numbers of astrocytes per patient that are sequenced, which
157 renders astrocytic datasets underpowered (discussed in (Liddelow, Marsh, & Stevens, 2020). The
158 second challenge is to analyze a sufficiently large number of subjects to ensure that patient
159 heterogeneity, a critical factor for drug development (Devi & Scheltens, 2018) manifests itself. The
160 studies performed by (B. Zhang et al., 2013) and (Neff, 2021) analyzed 1647 and 364 subjects,
161 respectively, whereas (Mathys et al., 2019) and (Grubman et al., 2019) examined only 48 and 12
162 subjects, including patients and controls. Only (Neff, 2021) reports molecular heterogeneity among
163 individuals with same clinical diagnosis, but astrocytic data are scarce.

164 The main goal of this study was to extract consensus astrocytic data from bulk transcriptomic data
165 from three large independent clinical AD databases, encompassing 766 subjects. 'Consensus data' was
166 defined as data detected in at least two out of the three databases. Identification of astrocyte-specific
167 genes was optimized by taking a reverse approach as compared to previous studies: instead of
168 determining *a posteriori* which self-organized gene modules might be astrocytic, we localized pre-
169 determined astrocytic gene clusters in whole-brain AD transcriptomes with two-dimensional
170 hierarchical clustering. The workflow is in **Fig. 1**. First, we classified brain genes as cell-specific or
171 non-specific using RNAseq data from astrocytes, neurons, microglia, endothelial cells and
172 oligodendrocytes isolated from aged healthy human brains (Y. Zhang et al., 2016), and a combination
173 of two algorithms: hierarchical clustering, and a recently proposed univariate cell-type enrichment τ
174 scoring (Kryuchkova-Mostacci & Robinson-Rechavi, 2017). Second, astrocytic and, for comparison,
175 neuronal genes were manually annotated according to functions, including cell-type specific functions.
176 Third, the gene clusters were localized in three AD whole-brain transcriptomes generated by the
177 Mount Sinai Hospital (MtSINAI) (B. Zhang et al., 2013) the Mayo Clinic (MAYO) (Allen et al., 2016),
178 and the Religious Order Study and the Rush Memory and Aging project (ROSMAP), which also
179 contains subjects diagnosed with MCI (Bennett et al., 2018). These databases present the advantages
180 of including large cohorts (78-219 subjects), which greatly facilitates the use of multivariate systems
181 approaches, and of having been generated by two different approaches, microarrays and RNAseq, thus
182 diminishing technique-associated bias. Finally, alteration of astrocytic and neuronal functional
183 categories in AD and MCI groups versus controls was statistically established using gene set variation
184 analysis (GSVA), and principal component analysis (PCA). We present the most comprehensive
185 transcriptomic analysis of human AD astrocytes to date using three independent cohorts. As
186 advocated in a recent consensus article about reactive astrocytes (Escartin et al., 2021), the impact of
187 pathway alterations suggested by omics was interpreted in the context of astrocyte biology, instead of
188 resorting to simplistic categorizations of astrocytes as 'neuroprotective' or 'neurotoxic' from the point
189 of view of neurons. In this vein, our analysis points to dysfunction of the endolysosomal
190 system/mitochondrion axis as a key driver of the phenotypical transformation of reactive astrocytes
191 in AD.

192 Material & Methods

193 Transcriptome datasets

194 The cell-type specific RNAseq datasets generated from healthy human brains (Y. Zhang et al., 2016)
195 were downloaded from the National Center for Biotechnology Information (NCBI) Gene Expression
196 Omnibus (GEO) under accession number GSE73721 pre-aligned to gene symbols by the authors using
197 human genome version 19. The database consisted of transcriptomic data from brain cells isolated

198 from temporal cortical lobes of juvenile (8-18 years old) and adult (21-63 years old) non-demented
199 individuals. Transcriptomes were included from 12 astrocytic, one neuronal, five oligodendrocytic,
200 three microglial, and two endothelial samples from individual patients (**Supplementary file 1,** tab
201 2). Principal component analysis (PCA, computed in R, R Foundation for Statistical Computing,
202 Vienna, Austria) revealed that transcriptomic data of astrocytes isolated from young (<47 years old)
203 and old (>47 years old) were separated along principal component 1 (PC1, **Supplementary file 1,**
204 tab 3). Since the goal of the study was to identify cell-specific signatures in aged subjects, data from
205 young individuals were discarded, retaining a total of six astrocyte transcriptomes from 47–63-year-
206 old subjects, together with all 11 transcriptomes from the remaining cell types. A threshold was set for
207 gene expression such that a given transcript should present a count > 1 in reads per kilo base per
208 million mapped reads (RPKM) in at least one sample. Genes with no counts > 1 were discarded from
209 the analysis. 11077 genes were above this threshold (**Supplementary file 1,** tab 4).
210
211 The MtSINAI database containing microarray data of samples from the prefrontal cortex of 101
212 controls and 129 AD patients obtained from the Harvard Brain Tissue Resource Center was
213 downloaded from GEO under accession number GSE44770 (B. Zhang et al., 2013). The Rosetta gene
214 identifiers were converted to the corresponding gene symbols using the Rosetta/Merck Human 44k
215 1.1 microarray platform table under accession number GPL4372. When multiple Rosetta identifiers
216 mapped to the same gene, the identifier with the greatest variance across samples was selected. The
217 MAYO database, which contains data from the temporal cortex of 78 control samples and 82 AD
218 samples, was downloaded from Synapse.org under Synapse ID syn3163039 (Allen et al., 2016). The
219 data were downloaded as MayoRNAseq_RNAseq_TCXCounts_normalized.tsv, pre-aligned to
220 Ensemble Gene Identifier. Ensemble Gene IDs were then converted to HGCN gene symbol using
221 `biomaRt` v. 2.32.1 in R (r-project.org). When multiple Ensemble Gene IDs mapped to the same gene
222 symbol, the one with greatest variance was selected. The ROSMAP database (Bennett et al., 2018)
223 contains data from the dorsolateral prefrontal cortex obtained from autopsied non-demented
224 individuals or patients diagnosed with AD. The data were downloaded from Synapse.org under
225 synapse ID syn8456629 as ROSMAP_DLPFC_netResidualExpression.tsv. The dataset contained 200
226 control cases, 157 MCI cases, and 219 AD cases. In the MCI group, there was no stratification into MCI
227 and MCI-AD. The dataset as posted by the authors had been adjusted via voom (mean-variance
228 modelling at the observational level) normalization to remove bias associated with batch number,
229 RNA integrity, and other data acquisition and processing co-variates. Missing transcript values in the
230 dataset were imputed using a nearest neighbor averaging method using the `impute` package in R.
231
232

Univariate cell-type enrichment score

To determine the cell-specificity of human genes listed in the brain-cell transcriptomics database (Y. Zhang et al., 2016), we used the τ method, reported to be particularly robust compared with other scoring approaches to identify tissue specificity of a gene among different magnitudes of expression and sizes of datasets (Kryuchkova-Mostacci & Robinson-Rechavi, 2017). The τ enrichment score was computed as:

$$\tau = \frac{\sum_{i=1}^{n}\left(1-\hat{x}_i\right)}{n-1}; \hat{x}_i = \frac{x_i}{\max_{1\le i\le n}\left(x_i\right)}$$

where x_i is the mean expression of the gene within i^{th} cell type and n is the number of cell types. We then define the cell type enriched in the gene as that with the greatest average expression among all cell types. Top τ scores per gene are in **Supplementary file 1**, tab 5. A score of $\tau \geq 0.8$ indicates that the gene is specific for a given cell type, and a score of $0.8 > \tau \geq 0.6$ that the gene is enriched in that cell type. For simplicity, henceforth we refer to genes with $\tau \geq 0.6$ as 'enriched', although note that the 'enriched' pool also includes specific genes. Finally, $\tau < 0.6$ indicates that the gene is non-specific, although it is assigned to the cell type with the greatest average expression.

Hierarchical clustering

The cell type specific data from (Y. Zhang et al., 2016) (**Supplementary file 1,** tab 4) were z-scored for each gene across samples. Gene and sample hierarchical clustering were conducted using a Euclidian distance measure, and the average agglomeration method in R. Gene clusters associated with neurons and astrocytes were determined by cutting the dendrogram at a height of 3.76 to achieve that at least 70% of the genes in the neuron and astrocyte clusters have the highest τ for that cell type (results from hierarchical clustering are in **Supplementary file 1**, tabs 6-8). Corresponding cell-specific gene clusters in whole tissue data sets (MtSINAI, MAYO, and ROSMAP) were identified by sorting the genes of whole-tissue data according to cell type specific datasets. Whole-tissue subject samples (columns) were then clustered within each Control, MCI, or AD cohort (Euclidian distance and Ward.D2 agglomeration) to identify molecularly-defined sub-groups of samples.

Data normalization within each cell type

A recognized caveat of bulk transcriptomic analyses is that DEG may reflect changes in cell-type composition rather than real changes in cell-specific transcriptomes. This is relevant to AD because there is neuronal death (Gomez-Isla et al., 1997), and microglia proliferation (Marlatt et al., 2014).

263 Since neurons are the most predominant cell type in the brain (40% in the human neocortex (Pelvig,
264 Pakkenberg, Regeur, Oster, & Pakkenberg, 2003)), a decrease of the neuronal pool, with no change in
265 the astrocyte pool (Marlatt et al., 2014), arguably results in the artificial up-regulation of astrocyte
266 genes. Several approaches have been employed to correct for cellular composition, such as use of
267 several of the so-called 'high fidelity' genes primarily expressed by one cell type (Kelley, Nakao-Inoue,
268 Molofsky, & Oldham, 2018). Here, we reasoned that reliance on a subset of highly cell-specific genes
269 could lead to artifacts should their expression change in the course of the disease, because there is no
270 assurance that they are stably expressed as house-keeping genes. Therefore, we elected to remove
271 gross variance by normalizing gene expression within the neuronal and astrocyte clusters according
272 to the shifts in distribution of differential expressions of all genes. This was accomplished by variance
273 stabilizing normalization using `limma` in R, which simultaneously correct each dataset for
274 dependence of variance on the mean. Removal of gross variance is widely-used in normalizations of
275 transcriptomic data, based on the premise that, since only a negligible proportion of genes have their
276 expression changed following perturbations (Lin, Du, Huber, & Kibbe, 2008), a bulk shift in the gene-
277 expression distribution in a given cell population reflects changes in the proportion of that cell type
278 among brain cell populations. Thus, correcting gene expression according to the shift would unmask
279 the real changes in gene expression. We applied this correction separately to the neuronal and
280 astrocytic gene clusters.
281

282 Cell function annotation and gene set variation analysis

283 Neuronal and astrocytic gene clusters generated by combining τ (Kryuchkova-Mostacci & Robinson-
284 Rechavi, 2017) and hierarchical clustering of transcriptomes from cells from healthy brains (Y. Zhang
285 et al., 2016), were organized in functional categories and subcategories (**Supplementary file 2**).
286 Categories were manually curated by one expert and cross-validated by another expert using
287 information from GeneCards, perusal of Medline and PubMed, and open-source platforms such as GO,
288 KEGG, and Reactome. Manual curation was indispensable for two reasons. First, over 60% of the
289 genes in the astrocytic cluster were not annotated in open-source platforms. This means a substantial
290 loss of usable gene data if we only relied on genes annotated in open-source platforms. Second,
291 annotation in such platforms represents 'canonical' pathways with little consideration for the fact that
292 different CNS cell types are molecularly and functionally distinct (Y. Zhang et al., 2016). This
293 limitation is critical for astrocytes. For example, unlike neuronal compartments such as 'synapses',
294 'dendrites' and 'spines', a highly specialized astrocytic compartment termed 'perisynaptic astrocyte
295 processes' (PAP), concentrating RNA transcripts related to glutamate and GABA metabolism, energy
296 metabolism, as well as the ribosomal machinery to perform local RNA translation (Sakers et al., 2017),
297 is not a category in current KEGG and GO databases. The genes were organized in general categories

298 and subcategories using a mixed set of criteria including general pathways (e.g. carbohydrate
299 metabolism or amino acid metabolism) and subcellular compartments with a clear functional
300 specialization (e.g. mitochondria, peroxisome or lysosome). Such flexibility allowed us to optimize
301 gene inclusion, while generating gene sets with sufficient numbers of genes for statistical purposes.
302 Although most genes were assigned to only one category, around 100 genes were assigned to two
303 categories (in blue, **Supplementary file 2,** tab 'astrocyte cluster 4'). The majority of those genes (96)
304 were PAP genes, because we reasoned that their presence in PAP does not exclude relevance in other
305 subcellular compartments. For example, *ALDOC* and *ACO2* are, plausibly, ubiquitous enzymes
306 relevant for general glycolysis and mitochondrial Tricarboxylic Acid (TCA) cycle throughout the cell.
307 Likewise, genes related to 'TNFalpha signaling' are in 'stress responses'/'cytokines' as well as in
308 'gliotransmission', for TNFalpha has been described to modulate glutamate exocytosis (Santello, Bezzi,
309 & Volterra, 2011). Overlap between groups was less than 5% with the exception of 'PAP and
310 gliotransmission': 17.8% genes in 'gliotransmission' were in 'PAP', and 10.3% of PAP genes were in
311 'gliotransmission'. For neurons, each gene was assigned to only one category.

312 Using our novel annotation database, the `GSVA` package in R was used to identify the enrichment of
313 each gene set across all samples. GSVA is a generalized gene set enrichment method that detects
314 variations of pathway activity over a sample population in an unsupervised manner (Hanzelmann,
315 Castelo, & Guinney, 2013). Statistical differences in enrichment scores for each gene set between
316 subject groups were computed by comparing the true differences in means against a null distribution
317 obtained by permuting the gene labels and re-computing the GSVA 1000 times. False discovery rate
318 adjust p-values (qFDR) were computed using the method of Benjamini & Hochberg (Hanzelmann et
319 al., 2013). Gene sets with FDR adjusted p value qFDR < 0.05 were considered significant.
320

321 Relationships between clinical stages and GSVA scores

322 The ROSMAP dataset includes Braak and CERAD (Consortium to Establish a Registry for Alzheimer's
323 disease) pathological scores, APOE genotype, and sex for each sample. To determine the relationship
324 between these phenotypes and the GSVA enrichment scores for each sample, we used the `stats` R
325 package to fit linear models between enrichment scores and either Braak or CERAD for each gene set.
326 The MAYO and MtSINAI databases do not include Supplementary information per subject other than
327 the clinical classification.

328

329 # Results

330 ## Hierarchical clustering identifies groups of cell-type specific genes

331 To identify astrocyte-specific genes, we calculated the metric τ (Kryuchkova-Mostacci & Robinson-
332 Rechavi, 2017) for every gene in the transcriptomes from isolated brain cell types generated by Zhang
333 et al. 2016 (**Supplementary file 1,** tab 5 'τ scores'). Cell type-specific (τ ≥ 0.8) and cell type-enriched
334 (τ ≥ 0.6) genes represented 30% and 60% of the 11,077 genes, respectively. Astrocytes (8%), microglia
335 (7.6%) and neurons (7.2%) present the largest percentage of cell-specific genes, whereas neurons (21%)
336 contained the largest pool of cell-enriched genes, followed by microglia (13.4%) and astrocytes (9.4%).
337 In contrast, endothelial cells and oligodendrocytes presented the lowest percentages of cell-enriched
338 (6%) and specific (3%) genes.

339 In parallel, because cell-specific functions are arguably performed by co-expressed genes (Weirauch,
340 2011), we reasoned that cell-type specific genes would be identified by clustering analysis. Thus, we
341 applied hierarchical clustering (**Methods**) to the cell-type specific dataset, generating 194 clusters
342 that contained between 1-1651 genes (**Fig. 2A**; **Supplementary file 1,** tab 6 'Hierarchical clustering'
343 and tab 7 'Cluster description'). We found that genes from the same cell type segregated together,
344 defining clusters of highly co-expressed genes, plausibly representing cell-specific functions. The
345 dendrogram height of hierarchical clustering was set to identify gene clusters that were highly
346 enriched for individual brain cell types. The criteria for 'enrichment' was that the cluster contained
347 more than 100 genes, of which over 70% corresponded to a unique cell type with τ ≥ 0.6
348 (**Supplementary file 1**, tab 8 'cluster selection'). Five clusters fulfilled these criteria, corresponding
349 to astrocytes (cluster # 4), endothelial cells (cluster # 5), neurons (cluster # 13), microglia (cluster #
350 17) and oligodendrocytes (cluster # 164). There were other clusters containing over 77% of total of
351 neuronal (e.g., clusters # 10, 116) or microglial (e.g., clusters # 30, 15) genes (**Supplementary file 1**,
352 tab 8 'cluster selection'), but they were excluded from the analysis because less than 54% of their genes
353 was enriched (τ ≥ 0.6) for that cell type, suggesting lower cell type specificity.

354 We continued with astrocyte cluster 4 (1651 genes) and neuronal cluster 13 (1258 genes) for two
355 reasons: (i) a cluster size of over 1000 genes is sufficient for functional categorization and gene set
356 analysis and (ii) since molecular changes in neurons are better characterized in AD than changes in
357 astrocytes, neurons served as a positive control to assure correct data mining.

358 In the neuronal cluster # 13, 99.9 % of the genes were neuronal according to τ score, of which 54.1%
359 of genes were neuron-specific (τ ≥0.8), meaning that they encode for proteins that perform functions
360 highly specific to neurons. Indeed, the top 10 ranked genes based on τ (τ > 0.98) were related to

361 neurotransmission (*SYNPR, GABRA1, CNR1, SYT1, GABRG2* and *GAD1),* regulation of membrane
362 potential (*KCN2*), microtubules (*INA),* and cell adhesion *(RELN*). The remaining 45.9% ($\tau < 0.8$) were
363 neuron-enriched or bulk genes plausibly supporting neuron-specific functions, since they were co-
364 expressed with neuron specific genes (**Supplementary file 1**, tab 8 'cluster selection';
365 **Supplementary file 2**, tab 2 'Neurons cluster 13').

366 In astrocyte cluster # 4, 80% of the genes were astrocytic according to τ (**Supplementary file 1**, tabs
367 7 and 8 'Cluster description' and 'Cluster selection'; **Supplementary file 2**, tab 'Astrocytes cluster
368 4'). Further, 30% had $\tau \geq 0.8$, including genes that encode typical astrocyte proteins such as *GFAP*
369 ($\tau = 0.95$), glutamine synthase (*GLUL*, $\tau = 0.95$), glutamate decarboxylase (*GLUD2*, $\tau = 0.91$),
370 glutamate transporters (*EAAT1/SLC1A3*, $\tau = 0.83$), lactate dehydrogenase (*LDHB*, $\tau = 0.91$), and
371 enzymes involved in mitochondrial fatty-acid oxidation (ACADVL, $\tau = 0.92$). Enriched genes with
372 τ between 0.6-0.8, or bulk genes below 0.6, arguably necessary for astrocyte functions, are the
373 aquaporins A*QP1* ($\tau = 0.739$) and *AQP4* ($\tau = 0.744$), and the chaperone clusterin *CLU* (τ =0.373),
374 which was identified by GWAS as a risk factor in AD (Han, Qu, Zhao, & Zou, 2018). These findings
375 indicated that the group of genes gathered in cluster #4 is relevant to astrocyte biology.

376 Identification of cell-type specific gene clusters in AD databases

377 We next searched for the astrocytic and neuronal gene clusters in gene expression data from three AD
378 whole-tissue transcriptomic databases (heatmaps of z-scores in **Fig. 2B).** Unexpectedly, hierarchical
379 clustering of subjects (columns) of each cohort revealed heterogeneity in groups with the same clinical
380 diagnosis. Subjects were divided in at least two molecular groups within the Control, MCI, and AD
381 cohorts across the three databases, as shown by the division of the dendrograms into two large groups
382 in each cohort. We refer to *type 2* subjects as those showing blue z-scores within the neuron gene
383 cluster, suggesting massive down-regulation of genes, as compared to *type 1* subjects, in which genes
384 with red z-scores predominated. Type 1 sub-cohorts included Control1, MCI1 and AD1, while *type 2*
385 included Control2, MCI2 and AD2. Numbers of Control1/Control2 patients were 33/45 in Mayo,
386 51/149 in ROSMAP, and 81/20 in MtSINAI. Numbers of AD1/AD2 patients were 28/54 in Mayo,
387 70/149 in ROSMAP, and 66/63 in MtSINAI. MCI1/MC2 numbers were 99/58 in ROSMAP. We note
388 that heterogeneity in MtSINAI data has been recently reported and replicated in ROSMAP (Neff,
389 2021).
390
391 The most profound down-regulation of genes within the neuronal gene cluster was observed in AD2.
392 Because down-regulation of neuronal genes due to loss of synapses and neuronal demise is a hallmark
393 of AD (Gomez-Isla et al., 1997), we reasoned that AD2 was advanced AD, and Control1 a *bona fide*
394 control composed of subjects that were neither demented, nor preclinical or pre-symptomatic at the

time of death. Control1 and AD2 thus appeared to be the extreme groups across the continuum of AD phenotypes, and were thus selected for further analysis.

Since our goal was to identify changes in astrocytic functions, it was critical to eliminate gross variability among samples within the astrocytic and neuronal gene clusters due to global changes in cell composition. To do so, we applied variance stabilizing normalization (**Methods**), which shifted the peaks of the distributions of differences in gene expression between AD2 and Control1 to zero (**Fig. 3A**). Prior to normalization, the distributions of gene-expression differences shifted to the left in the neuronal cluster, suggesting depletion of neurons in AD2, while the distribution of astrocytic genes shifted to the right, suggesting a relatively higher content of astrocytes in AD2. After normalization, the global downregulation of all neuronal genes in cluster # 13 in *type 2* groups was attenuated, but intra-cohort heterogeneity nevertheless persisted such that type 2 clusters presented prominent down-regulation of neuronal genes as compared to type 1 clusters (**Fig. 3B** and **Supplementary file 3**). In addition, new gene clusters that were previously masked were unraveled by hierarchical clustering. Thus, there were three neuronal (**Fig. 3B,** N-a, b, c), and four astrocytic gene subgroups (**Fig. 3B,** A-a, b, c, d) with opposite expressions patterns in *type 1* versus *type 2* subjects. For example, N-b genes were globally downregulated in AD2 and Control 2, as compared to Control 1 and AD1. Importantly, N-b contained genes related to synaptic function, including glutamatergic and GABAergic neurotransmission (e.g., *GABRB3; GABRB2; GAD1; PDYN; SYN2; GABRG2; SYN1 NAPB; GRIA2; SLC17A7; GRIK2*), supporting that this cohort is a *bona fide* AD. The normalized expression of cluster # 4 genes in the three AD databases is in **Supplementary file 4**.

Because the ROSMAP database included clinical covariate data, such as CERAD and Braak scores, APOE genotype and sex, we examined whether *type 1* or *type 2* sub-cohorts were associated with specific covariates to gain insight into why they were molecularly heterogeneous. We found that Braak and CERAD scores were significantly higher in AD groups than in Controls (**Fig. 3C**), confirming the clinical diagnosis. However, *type 1* and *type 2* subjects with the same clinical diagnoses did not significantly differ in their pathological stages according to CERAD and Braak scoring; nor were type 2 groups more enriched in *APOE4* subjects or females (**Fig. 3D**).

GSVA reveals altered functions in AD and MCI versus Control1

We next identified changes in astrocytic and neuronal functions using the normalized expression data. Because the majority of the astrocytic genes were not annotated in existing pathways in open-source databases, we manually curated the astrocytic cluster in 17 functional categories (gene sets) and 135 subcategories, and the neuronal cluster in 15 functional categories and 79 subcategories (**Methods**, **Supplementary file 2**).

431 GSVA was then used to compare the gene sets corresponding to different functional categories among
432 cohorts, yielding an enrichment score for each subject and gene set. We started by comparing the
433 extreme cases, AD2 and Control1, using two criteria. First, probability values were computed using a
434 permutation analysis across genes (cut-off for statistical significance was set at FDR-adjusted $q < 0.05$,
435 **Methods**). Second, we considered that a function was altered in AD2 as compared to Control1 if such
436 alteration was detected in at least two out of the three databases (consensus criterion).

437 For neurons, seven functions were altered in AD2 versus Control1 **(Fig. 4A,** statistics in
438 **Supplementary file 5,** extended graphs in **Supplementary file 6**): 'neurotransmission' and 'gene
439 expression' were altered in the three databases, and 'synaptic plasticity', 'regulation of membrane
440 potential', 'neural development', 'mitochondria' and 'stress response' in MAYO and ROSMAP, but not
441 MtSINAI. 'Synaptic plasticity', 'neurotransmission', 'neural development' and 'membrane potential'
442 were down-regulated, and 'gene expression', 'mitochondria' and 'stress response' up-regulated.
443 Among significantly different gene sets in MAYO and ROSMAP (**Fig. 4A**), Control 2 and MCI2
444 resembled AD2, and AD1 and MCI1 resembled Control1 (**Fig. 4B**). In MtSINAI, we found no
445 statistically significant difference between Control 1 and Control 2, and AD groups were similar,
446 although changes in AD2 were more dramatic, as compared to Control1 (**Fig. 4B**).

447 For astrocytes, five functions were altered in AD2 versus Control 1 (**Fig. 5A,** statistics in
448 **Supplementary File 5**): 'PAP', 'plasticity' 'stress response' were up-regulated in three/three
449 databases, 'mitochondria' was down-regulated in three/three databases, while 'endomembrane
450 system' was down-regulated in two/three databases. Because 'PAP' are specialized astrocyte-neuron
451 contacts and, hence, this category includes many genes related to gliotransmission, and since
452 'gliotransmission' was highly significantly changed in ROSMAP (qFDR<0.001), and trending in
453 MAYO (qFDR=0.07), henceforth 'PAP' and 'gliotransmission' were considered together. As with
454 neurons, Control2 and MCI2 showed the same direction of change as AD2 compared to Control1 (**Fig.**
455 **5B**). Likewise, enrichment of these gene sets in AD1 resembled Control1, particularly in MAYO and
456 ROSMAP, while AD1 appeared to be a milder version of AD2 in MtSINAI.

457 Co-variance of gene sets with one another and with pathological covariates

458 *Correlations between altered functions and pathological stages*. Since CERAD and Braak scores were
459 available for the ROSMAP data, we examined relationships between the enrichment of each gene set
460 and pathological stages by regressing enrichment scores for each gene set and sample against the
461 corresponding CERAD and Braak scores, regardless of clinical diagnoses (**Methods**). Data from all
462 the individuals in the three groups (control, MCI and AD) were used in the analysis. For neurons, we
463 found no correlation between Braak and CERAD stages for any of the seven top dysregulated
464 categories described in **Fig. 4A**. The p values for regressions with Braak/CERAD scores were:

465 'neurotransmission' (0.536/0.919), 'synaptic plasticity' (0.342/0.703), 'neural development'
466 (0.85/0.552), 'membrane potential' (0.794/0.479), 'gene expression' (0.55/0.563), 'mitochondria'
467 (0.357/0.254) and 'stress response' (0.548/0.755) **(Supplementary file 7).** The lack of correlation
468 can be interpreted to indicate similar gene dysregulation in all the stages, suggesting that neuronal
469 dysfunction is an early event in AD pathology such that it appears in subjects with no (i.e., Control2)
470 or incipient (i.e., MCI2) cognitive deficits, and low CERAD and Braak scores.

471 For astrocytes, of the five functions that were significantly altered in AD2 vs Control1 (**Fig. 5A**), the
472 following ones significantly correlated with Break/CERAD according to p-values: 'mitochondria'
473 (0.0000203/0.000742), 'stress response' and 'plasticity' (0.0768/0.00967) (**Supplementary file**
474 **8**). In contrast, 'PAP' (0.563/0.838), 'gliotransmission' (0.811/0.805), and 'endomembrane system'
475 (0.709/0.942) did not correlate with pathological stages, suggesting that, as we reasoned with neurons,
476 they represent early manifestations of alterations in astrocytic functions. For example, there is a
477 progressive decline in the expression of mitochondrial genes from CERAD 1 to 3 and from Braak 1 to
478 6, while the expression of genes involved in 'endomembrane system' is altered even before the
479 detection of cognitive deficits in patients.

480 *Correlations among altered functions*. We examined correlations among all neuronal and astrocytic
481 gene sets by regressing enrichment scores for each gene set against each other gene set. Hierarchical
482 clustering of correlation coefficients and adjusted p-values are in **Supplementary file 9** for
483 ROSMAP, MAYO, and MtSINAI. In neurons, the strongest direct correlations were among highly
484 related functions such as 'membrane potential', 'neurotransmission' and 'synaptic plasticity' in
485 neurons. Likewise, in astrocytes, the strongest correlations were between 'PAP' and 'gliotransmission'
486 (orange squares). The strongest anti-correlations point to intertwined changes between: (i)
487 morphological remodeling of PAP and loss of synaptic functions, and (ii) survival pathways included
488 in 'plasticity' in astrocytes (see below) and organelle dysfunction.

489 Alteration of functional subcategories in astrocytes

490 We next aimed to gain further insight into which factors drive the functional alterations in AD
491 astrocytes by searching for functional *subcategories* with statistically significant differences in
492 enrichment scores between AD2 and Control1 (qFDR< 0.05) in at least two out of three of the
493 databases (statistics in **Supplementary file 10**).

494 The category 'PAP' includes different categories related to morphology, metabolism and gene
495 expression. The consensus subcategory significantly upregulated was 'PAP morphology' (qFDR
496 <0.001, AD2 vs Control1, in MAYO and ROSMAP). Because PAP are specialized in the functional

497 refinement of adjacent synapses at a micro scale (Sakers et al., 2017), increased expression of PAP-
498 related genes in AD astrocytes may be a compensatory reaction to locally optimize synaptic functions.

499 Subcategories in 'Plasticity' include annotations associated with morphological remodeling (e.g.,
500 'adherens junction', 'ECM', 'cytoskeleton', 'ciliogenesis', 'TGFbeta signaling', 'metalloproteases'), and
501 pathways involved in brain development whose role in adult astrocytes is not well understood (e.g.,
502 'axon outgrowth', 'synaptogenesis, 'WNT signaling', 'hippo signaling', 'smoothened signaling',
503 'hedgehog signaling', 'homeobox signaling', 'notch signaling', 'FGF signaling', 'pluripotency', and 'glial
504 cell fate commitment'). Significantly dysregulated pathways were 'ECM', upregulated in the three
505 databases, and 'hippo signaling' and 'ciliogenesis' (i.e., the process of generation of a microtubule-
506 based and centriole-derived cilium whose function in astrocytes is unknown), respectively
507 upregulated and down-regulated in two databases—note that the fact that the general trend of a given
508 general category is towards up-regulation does not preclude that some of its subcategories are down-
509 regulated.

510 'Stress responses' includes 'AMPK signaling', 'antioxidant response', 'cell death', 'chaperone', 'DNA
511 repair', 'hypoxia', 'complement system' and 'cytokines'. No subcategory was dysregulated according to
512 qFDR in at least two databases. However, it is worth noting that 'TNFalpha', which is a subcategory of
513 'cytokines' as well as of 'gliotransmission', was significantly dysregulated in MAYO and ROSMAP, and
514 trending in MtSINAI (qFDR=0.093).

515 In 'endomembrane system', encompassing genes related to 'endoplasmic reticulum', 'Golgi', 'lysosome'
516 and 'vesicles', no single subcategories were significantly dysregulated, while in 'mitochondria', 'ETC'
517 and 'TCA cycle' were significantly downregulated in AD2 versus Control1 in three and two databases,
518 respectively. For 'ETC', qFDR=<0.001, <0.001, 0.012, <0.001 in MAYO, ROSMAP and MtSINAI. For
519 'TCA cycle', qFDR=<0.001, 0.39, 0.01 in MAYO, ROSMAP and MtSINAI. All in all, the dysregulated
520 subcategories in astrocytes point to alterations in mitochondrial respiration concomitant to
521 morphological remodeling.

522 PCA confirms main functional changes in AD astrocytes

523 GSVA was dependent on gene sets organized into pre-determined functions. Thus, we also used PCA
524 as an alternative, unsupervised approach to gain independent insight into the predominant functional
525 changes of AD astrocytes. First, we examined whether expression of genes contained in the astrocytic
526 cluster # 4 segregated cohorts in ROSMAP. PCA segregated the Control1, MC1 and AD1 groups to the
527 left, and the Control2, MCI2 and AD2 groups to the right, according to the principal component 1 (PC1,
528 horizontal axis, **Fig. 6A**). Violin plots of PC1 scores per group confirmed this tendency.

529 Second, we examined the functions performed by the proteins encoded by the top 50 dysregulated
530 genes in PC1, representing the maximally co-varying astrocytic genes (**Supplementary file 11**).
531 Mirroring our results with GSVA, genes related to 'plasticity' and 'PAP/gliotransmission' were over-
532 represented in the up-regulated portion, whereas genes related to 'endomembrane system', 'gene
533 expression', and 'signaling' were predominant in the down-regulated portion (**Fig. 6B**). Genes related
534 to 'mitochondria' and 'stress responses' appeared in both sections, indicating mixed direction of
535 dysregulation in these functions. Unlike GSVA, PCA also detected changes in 'signaling', as suggested
536 by the presence of genes related to this function in the up and down segments of the top PC1 genes.

537 Third, we asked if the changes detected in AD astrocytes in ROSMAP with PCA were reproducible.
538 Thus, we determined the capacity of the PC1 genes to segregate cohorts in MAYO and MtSINAI. As in
539 ROSMAP, Control1 subjects were mostly negative, and AD2 cases were mostly positive in MAYO and
540 MtSINAI, thus validating the discriminating capacity of the maximally co-varying genes in PC1 (**Fig.
541 6C**). AD1 segregated with Control 1 in MAYO, but not in MtSINAI, where AD1 aligned with AD2,
542 confirming less intra-cohort heterogeneity in MtSINAI than in the other two databases, as shown with
543 GSVA. Altogether, these results point to multi-factorial changes in AD astrocytes, encompassing
544 changes in astrocyte-neuron interactions and organelle dysfunction (model in **Fig. 7A** and description
545 in **Discussion**).

546 Comparison with other human studies

547 Comparisons among our study and snRNAseq and whole-tissue transcriptomic studies (Mathys et al.,
548 2019; B. Zhang et al., 2013) (Grubman et al., 2019) are in (**Supplementary file 11**). The greatest
549 concordance was found between our study and (B. Zhang et al., 2013). Thus, there was an 11% overlap
550 between cluster # 4 and Zhang data. Importantly, 94.9 % of the common genes were localized in the
551 UP portion of the PC1 list, representing 28% of such list, and they were particularly enriched in the 50
552 Top UP PC1 (50% overlap with Zhang's list). Common genes were related to 'Gliotransmission' (e.g.,
553 glutamate transporter *SLC1A3*), 'Plasticity' (e.g., Hippo Signaling *TP53BP2*), 'Stress response '(e.g.,
554 antioxidant *PON2*), and 'Mitochondria' (e.g., amino acid metabolism *HADHB*). By contrast, there was
555 scarce representation of astrocytic genes from (B. Zhang et al., 2013) in the down-regulated portion of
556 our cluster 4, where the majority of the genes related to mitochondrial metabolism and the
557 endolysosomal system lie. Since the Zhang astrocytic cluster was generated by co-expression within
558 AD transcriptomes, we reason that down-regulated astrocytic genes may not co-express any longer
559 with up-regulated ones. In summary, our study confirms the relevance of glutamate and amino acid
560 metabolism in AD pathogenesis reported in large-scale network analysis (B. Zhang et al., 2013), and
561 links it to organelle dysfunction, particularly that of mitochondria, which, as noted, presented a
562 marked negative correlation with pathological stages according to the regressions with Braak/CERAD

563 scores (p-value 0.0000203/0.000742, **Supplementary file 8**). As to scRNASeq studies, 12.7% and
564 1.1% of Cluster # 4 overlap with astrocytic DEG (Grubman et al., 2019; Mathys et al., 2019),
565 respectively (**Supplementary file 11**). Comparison of the top 50 UP and 50 DOWN PC1 genes
566 reveals little concordance: as compared to the 50% of top 50 PC1 genes found in (B. Zhang et al., 2013),
567 only 0.3% and 1.3% of top 50 PC1 genes are annotated in the DEG in (Mathys et al., 2019) and
568 (Grubman et al., 2019). Of note, (Mathys et al., 2019) and (Grubman et al., 2019) only share 32 genes,
569 representing 47% of the DEG in (Mathys et al., 2019) and 4.5 % of those in (Grubman et al., 2019).
570 Further, only 2.3% and 14.6% of the astrocytic cluster from (B. Zhang et al., 2013) overlap with
571 (Mathys et al., 2019) and (Grubman et al., 2019). The incomplete equivalence among databases may
572 be due to several factors, including: (i) differences in methodologies, (ii) classifications of disease (e.g.,
573 clinical in (B. Zhang et al., 2013), (Grubman et al., 2019) and our study, but associated to amyloid-β
574 pathology in (Mathys et al., 2019) regardless of clinical diagnosis), (iii) brain regions sampled
575 (prefrontal or temporal cortex in (Mathys et al., 2019) (B. Zhang et al., 2013) and in our case, but
576 entorhinal cortex in (Grubman et al., 2019)), and/or (iv) the total number of subjects analyzed (1647
577 in (B. Zhang et al., 2013), 48 in (Mathys et al., 2019), 12 in (Grubman et al., 2019), and 766 herein.
578

579 ## Cortical APP/PS1 astrocytes partially mimic cortical AD astrocytes

580 We finally asked whether changes identified in cortical AD astrocytes are recapitulated in mouse
581 models. To answer this question, we examined the expression of human astrocytic genes from cluster
582 #4 in the transcriptome of cortical astrocytes isolated from 15-18 month-old APP/PS1 versus WT mice
583 (N=4 per group) (Orre et al., 2014), using the same functional categorization and statistical tools
584 utilized for human AD astrocytes. Comparison with recent snRNAseq mouse data (Habib et al., 2020),
585 is not appropriate since this study was carried in hippocampi. We found robust down-regulation of
586 all human astrocytic functions in APP/PS1 cortical astrocytes (**Fig. 7B**). Thus, APP/PS1 astrocytes
587 mimic the down-regulation in 'endomembrane system' and 'mitochondria' detected in AD astrocytes,
588 but not the up-regulation of 'PAP', 'stress responses' and 'plasticity'. We also compared the top 50 and
589 bottom 50 DEG from APP/PS1 astrocytes (Orre et al., 2014) with the top 50 and bottom 50 genes
590 from PC1 in human AD astrocytes (**Fig. 6B**). GSVA confirmed that both the top and bottom human
591 AD astrocyte gene sets were down-regulated in APP/PS1 mice (**Fig. 7C**, left). Importantly, the pool of
592 immune-related genes reported to be up-regulated in mouse APP/PS1 astrocytes (Orre et al., 2014)
593 are predominantly microglial according to τ scores , and, with the exception of *C1S,* do not coincide
594 with functionally related human astrocyte-enriched genes in cluster # 4 subcategories such as
595 'cytokines' and 'complement' (**Supplementary file 12**). As also concluded in (Orre et al., 2014), this
596 divergence points to the existence of two distinct gene pools in cortical APP/PS1 astrocytes that change
597 in opposite directions in advance disease stages: a down-regulated pool of typical homeostatic

598 astrocyte genes, and an up-regulated pool of typical microglia genes. The loss of astrocytic functions
599 and the adoption of a microglia-like phenotype suggests that cortical APP/PS1 astrocytes may undergo
600 a phenotypical involution with time.

601 Finally, regardless of the direction of change in mice, DEG in APP/PS1 vs WT cortical astrocytes were
602 largely up-regulated in AD2 the three human databases (**Fig. 7C**, right panels). This suggests
603 predominance of typical microglial genes in advanced AD, plausibly upregulated in both microglia and
604 astrocytes.

605

606 # Discussion

607

608 Because of the challenges associated with the isolation of astrocytes or their nuclei, and to profit from
609 the wealth of large publicly available human datasets, the goal of this study was to gain insight into
610 what happens to astrocytes in AD using whole-brain transcriptomes and systems-biology tools. The
611 approach consisted of re-compartmentalizing whole-brain transcriptomes from Control, MCI and AD
612 subjects into contributions from individual cell types by using pre-clustered cell-specific gene sets.
613 The study has four main findings. First, GSVA and PCA show that AD astrocytes—so defined because
614 they appear in patients with the typical down-regulation of neuronal synaptic functions documented
615 in AD—undergo a profound phenotypical transformation encompassing down-regulation of genes
616 encoding for organelle proteins, and up-regulation of genes related to PAP, gliotransmission, plasticity
617 and stress responses. Second, unbiased hierarchical clustering of patient cohorts reveals major intra-
618 cohort heterogeneity, i.e., relationships are not robust between gene profiles, clinical diagnosis, and
619 pathological stage according to CERAD and Braak scoring, as recently reported in (Neff, 2021). In
620 other words, some non-demented subjects present AD-like astrocytes and neurons, while some
621 demented subjects present healthy ones, particularly in MAYO and ROSMAP. Third, according to
622 regression analyses between functions and CERAD or Braak scores, some astrocytic functions may be
623 altered early in the AD continuum (e.g., PAP, gliotransmission and endomembrane system), while
624 other functions may be increasingly dysregulated in parallel with the deposition of neuritic plaques
625 and neurofibrillary tangles (e.g., mitochondrial functions, plasticity-related pathways and stress
626 responses). Fourth, multivariate statistics and hierarchical clustering show that cortical astrocytes
627 from human AD and from a 15–18-month-old mouse model of ADAD (Orre et al., 2014) are distinct
628 transcriptional entities.

629

630 ## Limitations

631 A limitation of our study is that pathway dysregulation during AD may result in the remodeling of cell-
632 type specific gene clusters, such that gene clusters identified in healthy brain transcriptomes may no

633 longer exist in AD. However, quantification of network reorganization in AD subjects using a metric
634 called modular differential connectivity (MDC) showed equal or enhanced connectivity in 95.5% of
635 the modules (B. Zhang et al., 2013), suggesting that clusters identified by co-expression analyses in
636 healthy cells are, for the most part, preserved in AD. Nevertheless, we recognize that our analysis may
637 overlook changes in transcripts ubiquitous in all cell types, e.g., glycolysis related transcripts. It may
638 also overlook upregulation in astrocytes of transcripts typical of non-astrocytic cells, namely microglia,
639 including the inflammation-like response common to astrocytes and microglia, as described in 15-18-
640 month-old APP/PS1 transgenic mice (Orre et al., 2014). Conversely, our analysis may detect down-
641 regulated astrocytic genes (e.g., mitochondrial genes) that may go unnoticed in large-scale clustering,
642 for their expression changed in opposite directions to the majority of genes in the original cluster (B.
643 Zhang et al., 2013). Still, our results may be just the tip of the iceberg in terms of defining the totality
644 of changes in human AD astrocytes.
645
646 Yet another limitation of the analysis is that it does not reveal astrocyte populations, recently described
647 in a mouse model of AD using snRNAseq (Habib et al., 2020), although it is tempting to speculate that
648 the four astrocytic gene clusters identified in the clinical cohorts (**Fig. 3**) might represent distinct
649 transcriptomic states. Further, because transcriptomic data are cross-sectional and descriptive, they
650 do not demonstrate cause-effect relationships between pathway dysregulation and pathology, or
651 unequivocally prove that changes are adaptive (meant to compensate for dysregulated functions and
652 maintain or restore homeostasis), maladaptive (irreversibly contributing to dyshomeostasis and
653 neurodegeneration), or epiphenomena with scarce bearing on disease onset and progression. Finally,
654 genetic data does not directly inform about changes in proteins and metabolites. Hence, predictions,
655 based upon these data (below) need validation in appropriate models.
656

657 Key implications and predictions

658 *Use of molecular data for subject stratification in clinical trials*. Neurocognitive measurements,
659 atrophy patterns assessed with neuroimaging, neurofibrillary tangles assessed *postmortem*, CSF
660 levels of amyloid-β1-42 and Tau, as well as Tau neuroimaging, have revealed subtypes of AD (Devi &
661 Scheltens, 2018; Dujardin et al., 2020). This clinical and biological heterogeneity, which is
662 increasingly recognized to be a major obstacle to establishing drug efficacy in clinical trials, starts to
663 be addressed with molecular tools, as shown by the recent detection of three molecular classes in an
664 extended MtSINAI cohort using RNAseq transcriptomics in four brain regions (Neff, 2021). They
665 found the largest global change in the parahippocampal gyrus (PHG), presenting three molecular
666 subtypes among subjects, termed A, B and C. Although our analysis was performed in cortical samples
667 rather than the PHG, we reason that our AD2 group might correspond to what they called 'C typical'
668 AD class, and our AD1 might correspond to what they called the 'A atypical' AD class. The reason is

669 that both AD2 and C present downregulation of synaptic networks as compared to AD1 and A. No
670 further comparison between our study and (Neff, 2021) can be performed with regards to astrocytes
671 because, among only three genes reported to be upregulated in astrocytes in the 'C typical AD class',
672 only *GNA12* appears in our astrocytic cluster # 4—although it is indeed upregulated in ROSMAP
673 (**Supplementary data 13**).
674
675 A disconnect between presence of AD pathology and cognition has been long recognized
676 (Neuropathology Group. Medical Research Council Cognitive & Aging, 2001). The terms 'resistance'
677 and 'resilience' have been coined to describe two distinct clinical scenarios consisting of avoiding
678 pathology ('resistance') *versus* coping with pathology ('resilience') (reviewed in (Arenaza-Urquijo &
679 Vemuri, 2018)). Thus, resistant subjects would be cognitively normal without significant Abeta or Tau
680 pathology despite being at high-risk, considering several factors including age or APOE genotype. By
681 contrast, resilient subjects would remain cognitively normal despite significant AD pathology. We
682 speculate that our AD1 subjects were perhaps 'resilient' to AD pathology, which they had, according
683 to high CERAD and Braak scores, but that they developed dementia due to comorbidities (e.g., Lewy
684 bodies, vascular disease, TDP43 deposits). However, the possibility exists that the tissues used for
685 transcriptomic analysis and neuropathological assessment of neuritic plaques and neurofibrillary
686 tangles were not the same. This means that the transcriptomic analysis in demented AD1 subjects with
687 a healthy-like molecular profile might have been performed in cortical tissue spared from ongoing
688 pathology, such that AD1 subjects were not truly resilient. By contrast, regardless of how omics and
689 neuropathological assessments were performed, Control2 subjects in ROSMAP and MAYO with an
690 AD-like molecular profiles were cognitively normal. Thus, Control2 subjects might be high-risk, pre-
691 symptomatic, resistant subjects in whom the appearance of neuritic plaques, Tau tangles, and
692 cognitive impairment, was delayed despite the decreased expression of synaptic genes, plausibly
693 caused by soluble oligomeric amyloid-β (Marsh & Alifragis, 2018). Whatever the case, our study
694 supports the use of omics-based molecular phenotyping and clustering statistics as unbiased tools to
695 stratify patients in clinical trials in the spirit of personalized medicine.

696 *Early dysregulation of the endolysosomal system in astrocytes*. The category 'endomembrane system'
697 was found down-regulated in AD2 vs Control1 by GSVA. Further, genes related to endoplasmic
698 reticulum (e.g., *FAF2, PIGX*), endocytosis (e.g., *ATXN2, MEGF8, RAB11FIP2*), and autophagy
699 (*ATG9A*) ranked among the top50PC1 downregulated in ROSMAP (**Fig. 6B**), and were significantly
700 down-regulated in at least two of the three databases by Wilcoxon test (**Supplementary file 4**).
701 These findings support cumulative evidence in mouse and *in vitro* models of AD pointing to inefficient
702 phagocytosis and degradation of amyloid-β protofibrils (Funato et al., 1998; Sanchez-Mico et al., 2020;
703 Sollvander et al., 2016) and dystrophic neurites (Gomez-Arboledas et al., 2018) by astrocytes, as well

704 as decreased exosome production from astrocytes (Abdullah et al., 2016). Thus, our study and others
705 do not support the notion that astrocytes efficiently clear amyloid-β plaques, as initially suggested by
706 evidence in non-primary cultured astrocytes (Wyss-Coray et al., 2003), which, arguably, are endowed
707 with greater motility and morphological plasticity than primary or *in situ* astrocytes. Moreover,
708 targeted enhancement of lysosomal biogenesis by overexpression of the transcription factor EB (TFEB)
709 in astrocytes enhances Tau clearance, and reduces pathological hallmarks in the hippocampus of PS19
710 tauopathy mice (Martini-Stoica et al., 2018), suggesting that the improvement of lysosomal function
711 in astrocytes may also reverse Tau pathology in AD. Along these lines, TFEB has been reported to
712 regulate AD risk genes in an astrocyte subpopulation detected in AD brains by snRNAseq (Grubman
713 et al., 2019).

714 *Early and concomitant alteration of neuronal-astrocyte contacts*. This prediction is based on two
715 findings: the inverse correlation of changes in synaptic functions and PAP, and the lack of correlation
716 between these functional categories with pathological stages, suggesting that they change early in AD.
717 Accordingly, both PAP and synaptic genes are dysregulated in non-demented subjects with a *type 2*
718 molecular profile (Control2), which, as noted earlier, may represent preclinical AD. Specifically, GSVA
719 showed up-regulation of 'PAP morphology', whose leading gene *EZR* encodes ezrin, a protein involved
720 in PAP motility and in the anchoring of the astrocyte membrane to neurons or the extracellular matrix
721 (Derouiche & Geiger, 2019). Also, genes related to integrin and cell motility (e.g., *FERMT*2, *PREX2*)
722 were part of the top genes detected by PCA as defining AD astrocytes (**Fig. 6B**). We posit that
723 upregulation of PAP genes is an adaptive change to improve the coverage of neurons to counteract the
724 down-regulation of synaptic elements directly caused by oligomeric amyloid-β (Marsh & Alifragis,
725 2018). This scenario is supported by the upregulation of genes encoding for synaptogenic factors such
726 as thrombospondin and glypicans (*THSD1, GPC4*) in the three databases (**Supplementary file 4**).
727
728 *Mitochondrion dysfunction in AD astrocytes may impact gliotransmission*. It is generally assumed
729 that the well-established mitochondrion dysfunction (Swerdlow, 2018) and reduced glucose
730 metabolism in AD (often referred to as 'hypometabolism' (Hoffman et al., 2000)) are neuronal
731 phenomena. However, our analysis reveals down-regulation of nuclear-encoded mitochondrial genes
732 encoding TCA cycle and ETC components in astrocytes, suggesting deficiencies in energy-generating
733 mitochondrial pathways. For example, one of the consensus downregulated genes, *ATPAF1*, is a
734 component of the ATP synthase (complex V), and it is known that impairment of the ETC beyond
735 complexes I-III increases reactive-oxygen species formation while decreasing ATP formation (Shi &
736 Gibson, 2007). Moreover, i*n vitro* and *ex vivo* studies link mitochondrial dysfunction in astrocytes to
737 amyloid-β. Thus, in co-cultures of rat hippocampal neurons and astrocytes, amyloid-β causes loss of
738 mitochondrial potential and transient mitochondrial depolarization, concomitant to activation of

739 NADPH oxidase and decrease glutathione production, in astrocytes, but not neurons (Abramov,
740 Canevari, & Duchen, 2004). Loss of membrane potential and depolarization of astrocytic
741 mitochondria is prevented by antioxidants, and by the use of glutamate by mitochondrial complex I
742 as a substrate, suggesting that amyloid-β-elicited mitochondrial dysfunction is caused by oxidative
743 stress and deficits in substrate supply (Abramov et al., 2004). Interestingly, the mitochondrial
744 glutamate transporter *SLC25A18*, as well as the plasma membrane glutamate transporters *SLC1A3*
745 and *SLC7A11* are up-regulated in the three databases, and *SLC6A11* in two (**Supplementary file 4**),
746 suggesting that AD astrocytes recycle glutamate to counteract the damage caused by amyloid-β to
747 astrocytic respiration by increasing the supply of fuels amenable for oxidation. Along these lines,
748 *HADH8,* which encodes for an enzyme involved in mitochondrial beta oxidation, was found
749 upregulated in AD astrocytes by PCA.
750
751 Likewise, the consensus upregulation in AD astrocytes of the monoamine oxidase *MAO-B*, a
752 dopamine-degrading enzyme located in the outer mitochondrial membrane, may be interpreted as an
753 attempt to reverse respiratory deficits. This is supported by the recent discovery that MAO-B increases
754 the polarization of the inner mitochondrial membrane and ATP production by shuttling electrons
755 through the inter-membrane space (Graves et al., 2020). MAO-B upregulation in AD is relevant for
756 two reasons. First, the MAO-B ligand (11)C-deuterium-L-deprenyl may serve as a PET-based
757 biomarker of early astrocyte dysfunction in AD, as documented in ADAD (Rodriguez-Vieitez et al.,
758 2016). Second, MAO-B may affect the excitatory/inhibitory balance of neural circuits by producing
759 GABA from putrescine, as shown in APP/PS1 mice (Jo et al., 2014). In support of this scenario, the
760 genes encoding the GABA transporter *SLC6A11/GAT3*, which may extrude GABA coupled to
761 glutamate uptake, and *SLC7A2*, which imports the putrescine precursor L-arginine, are consensus
762 dysregulated genes (**Supplementary file 4).** Taken together, the data support that impaired
763 mitochondrial respiration in astrocytes switches gliotransmission to a GABA-dominant mode. A
764 detrimental effect of astrocytic GABA has been proposed based on the beneficial effects of the MAO-
765 B inhibitor selegiline on electrophysiological readouts in APP/PS1 mouse hippocampi (Jo et al., 2014);
766 however, there is no benefit of selegiline in patients (Birks & Flicker, 2003), thus raising doubts as to
767 whether APP/PS1 mice appropriately model the impact of astrocytic GABA in AD. Alternatively,
768 astrocytic GABA might counteract the loss of GABAergic tone that has been causally related with
769 neuronal hyperactivity, desynchronization of neural circuits, and amyloid-β production (Lee,
770 Gerashchenko, Timofeev, Bacskai, & Kastanenka, 2020). Since our regression analyses reveal that
771 mitochondrial dysregulation in astrocytes progressively increases in advanced pathological stages,
772 and since the upregulation of MAO-B detected by PET in the prodromal stages in ADAD is transient
773 (Rodriguez-Vieitez et al., 2016), we reason that the two strategies used by mitochondria to preserve

774 membrane potential and ETC (i.e., enhanced supply of substrates such as aromatic amino acids like
775 glutamate, and of electrons *via* MAO-B) eventually fail in astrocytes. As a consequence, glutathione
776 production might be decreased and NADPH oxidase activity increased (Shi & Gibson, 2007), perhaps
777 exacerbating oxidative stress and overall astrocyte malfunction in advanced AD.
778
779 *Pathological-stage dependent upregulation of 'plasticity' and 'stress response' pathways might*
780 *explain why, unlike neurons, astrocytes survive in AD.* The progressive upregulation of the
781 subcategory 'ECM', which includes integrins and proteoglycans, is not surprising considering the
782 indisputable adoption of a 'reactive' morphology by astrocytes in AD, consisting of engrossment of
783 primary and secondary processes due to over-expression of the intermediate filament protein GFAP,
784 and increased production of ECM proteins (Escartin, Guillemaud, & Carrillo-de Sauvage, 2019). More
785 intriguing is the consensus up-regulation of hippo signaling, an evolutionarily conserved network with
786 a central role in the regulation of cell proliferation, cell fate, organ growth and regeneration (Misra &
787 Irvine, 2018), and no reported role in healthy adult astrocytes, despite the fact that some of the genes
788 in this pathway are highly specific to human adult astrocytes according to τ (e.g., *WWC1* τ=0.91;
789 *WWOX* τ =0.86, and *YAP1* τ=0.88). *YAP1* was, moreover, detected by PCA as a relevant gene in the
790 astrocytic phenotype in AD. The upregulation of hippo signaling in AD astrocytes, as well as the global
791 upregulation of genes involved in brain development may be a manifestation of the well documented
792 phenomenon of re-activation of developmental pathways in reactive astrocytes that some authors
793 interpret as a failed attempt at reprogramming into neural stem cells (Torper & Gotz, 2017), and we
794 interpret to be a protective response to facilitate the survival of defective astrocytes. In addition, the
795 recent observation that *YAP1* regulates scar-border formation in spinal cord injury in mice (Xie et al.,
796 2020), suggests that hippo signaling is coordinated with the increased production of ECM in AD
797 astrocytes. Finally, the consensus dysregulation of the subcategory 'TNF-alpha' (**Supplementary**
798 **file 10**), and the consensus upregulation of *TNFRSF11B, TNFSF13 and TRAF3IP2*, members of the
799 IL17 family (*Il17D, IL17RB, and IL17RD*), and complement factors (*CD59, C1S*) (**Supplementary**
800 **file 4**) might be interpreted as detrimental 'neuroinflammation', but evidence supports modulatory
801 or protective actions of these factors (Masgrau, Guaza, Ransohoff, & Galea, 2017). First, TNFα may
802 facilitate the release of glutamate by improving vesicle docking at the astrocyte plasma membrane
803 prior to exocytosis (Santello et al., 2011), such that TNFα signaling may help adjust gliotransmission
804 in AD astrocytes. Second, the finding that Nrf2/IL17D axis acts as an antioxidant protective pathway
805 in stress responses induced by tumorigenic stimuli and viral infections (Saddawi-Konefka et al., 2016),
806 supports an astroprotective role of members of the IL17 family in AD. Also, members of the
807 complement system have been shown to facilitate amyloid-β phagocytosis (Iram et al., 2016).
808

Model of the phenotypical transformation of cortical astrocytes in AD

The key predictions from our analysis are summarized in **Fig. 7A.** We posit that amyloid-β drives the phenotypical change of astrocytes in AD in several stages by causing dysfunction of the endolysosomal/mitochondrial axis, which, in turn, prompts a change in the balance of excitatory/inhibitory neurotransmission. Impairment of mitophagy due to endolysosomal malfunction may further exacerbate mitochondrial dysregulation. Control2 subjects (cognitively normal/AD-like molecular profile) would be at stage a, and AD2 patients (demented, AD molecular profile) at stage b. In both a and b, the phenotypical change is complex and *mixed* with regards to possible clinical impact, for changes that may disrupt homeostasis of astrocytes themselves and/or astrocyte-neuron communications coexist with changes that may protect astrocytes and/or their interactions with neurons. The model thus represents a departure from simplistic neuroprotective/neurotoxic classifications of reactive astrocytes from the point of view of neurons. As recently discussed (Escartin et al., 2021), an 'astrocyte-centric' stance focused on the clarification of the maladaptive or adaptive nature of pathway changes in the complex astrocyte biology should be adopted. What is then the *net* impact of the mixed functional changes of reactive astrocytes on AD? In short, we posit that, despite organelle dysfunction, astrocytes manage in early disease stages to partially preserve their functions, including the modulation of neural circuits, through adaptive changes, while they become globally malfunctional in advanced stages. Thus, the early changes in astrocyte-neuron interplay may delay the onset of clinical symptoms, while detrimental phenomena would prevail in stage b. If these predictions are correct, therapies aimed at protecting and restoring the functions of the endolysosomal system and mitochondria to halter the transformation of astrocytes to stage b might help arrest the progression of AD. Even if GABA were detrimental, as reported in (Jo et al., 2014), preservation of mitochondrial respiration is therapeutically indicated, because increased GABA production, whatever its effect, would be the result of mitochondrial impairment. In summary, the present study points to prevention of organelle dysfunction in astrocytes as a therapeutic strategy in AD. These predictions need to be tested in transgenic mice or human cellular models that appropriately recapitulate the complex transformation of astrocytes in the AD continuum.

Conclusions

Our novel systems-biology based identification of astrocytic clusters in three independent datasets, encompassing 766 patients, represents the most comprehensive transcriptomic analysis of human astrocytes in AD to date. We highlight that manually curated functional annotations were implemented to circumvent deficits in astrocyte-specific annotations in current platforms. Further, molecular heterogeneity of subjects with the same clinical diagnosis was detected by hierarchical clustering and controlled for by performing independent statistics. The findings have led to a model

844 of stage-dependent astrocyte dysfunction in AD caused by Aβ-elicited damage of the endolysosomal
845 and mitochondrial systems. If this model is correct, astrocyte-targeted therapies aimed to prevent
846 organelle malfunction in astrocytes may be beneficial for AD.

847

848 **References**

849 Abdullah, M., Takase, H., Nunome, M., Enomoto, H., Ito, J., Gong, J. S., & Michikawa, M.
850 (2016). Amyloid-beta Reduces Exosome Release from Astrocytes by Enhancing JNK
851 Phosphorylation. *J Alzheimers Dis, 53*(4), 1433-1441. doi:10.3233/JAD-160292
852 Abramov, A. Y., Canevari, L., & Duchen, M. R. (2004). β-Amyloid Peptides Induce
853 Mitochondrial Dysfunction and Oxidative Stress in Astrocytes and Death of Neurons
854 through Activation of NADPH Oxidase. *The Journal of Neuroscience, 24*(2), 565-575.
855 doi:10.1523/jneurosci.4042-03.2004
856 Allen, M., Carrasquillo, M. M., Funk, C., Heavner, B. D., Zou, F., Younkin, C. S., . . . Ertekin-
857 Taner, N. (2016). Human whole genome genotype and transcriptome data for
858 Alzheimer's and other neurodegenerative diseases. *Sci Data, 3*, 160089.
859 doi:10.1038/sdata.2016.89
860 Arenaza-Urquijo, E. M., & Vemuri, P. (2018). Resistance vs resilience to Alzheimer disease:
861 Clarifying terminology for preclinical studies. *Neurology, 90*(15), 695-703.
862 doi:10.1212/WNL.0000000000005303
863 Bennett, D. A., Buchman, A. S., Boyle, P. A., Barnes, L. L., Wilson, R. S., & Schneider, J. A.
864 (2018). Religious Orders Study and Rush Memory and Aging Project. *J Alzheimers Dis,*
865 *64*(s1), S161-S189. doi:10.3233/JAD-179939
866 Birks, J., & Flicker, L. (2003). Selegiline for Alzheimer's disease. *Cochrane Database Syst*
867 *Rev*(1), CD000442. doi:10.1002/14651858.CD000442
868 Derouiche, A., & Geiger, K. D. (2019). Perspectives for Ezrin and Radixin in Astrocytes:
869 Kinases, Functions and Pathology. *Int J Mol Sci, 20*(15). doi:10.3390/ijms20153776
870 Devi, G., & Scheltens, P. (2018). Heterogeneity of Alzheimer's disease: consequence for drug
871 trials? *Alzheimers Res Ther, 10*(1), 122. doi:10.1186/s13195-018-0455-y
872 Dujardin, S., Commins, C., Lathuiliere, A., Beerepoot, P., Fernandes, A. R., Kamath, T. V., . . .
873 Hyman, B. T. (2020). Tau molecular diversity contributes to clinical heterogeneity in
874 Alzheimer's disease. *Nature Medicine, 26*(8), 1256-1263. doi:10.1038/s41591-020-
875 0938-9
876 Escartin, C., Galea, E., Lakatos, A., O'Callaghan, J. P., Petzold, G. C., Serrano-Pozo, A., . . .
877 Verkhratsky, A. (2021). Reactive astrocyte nomenclature, definitions, and future
878 directions. *Nat Neurosci*. doi:10.1038/s41593-020-00783-4
879 Escartin, C., Guillemaud, O., & Carrillo-de Sauvage, M. A. (2019). Questions and (some)
880 answers on reactive astrocytes. *Glia, 67*(12), 2221-2247. doi:10.1002/glia.23687
881 Funato, H., Yoshimura, M., Yamazaki, T., Saido, T. C., Ito, Y., Yokofujita, J., . . . Ihara, Y.
882 (1998). Astrocytes containing amyloid beta-protein (Abeta)-positive granules are
883 associated with Abeta40-positive diffuse plaques in the aged human brain. *Am J*
884 *Pathol, 152*(4), 983-992. Retrieved from
885 https://www.ncbi.nlm.nih.gov/pubmed/9546359
886 Gomez-Arboledas, A., Davila, J. C., Sanchez-Mejias, E., Navarro, V., Nunez-Diaz, C., Sanchez-
887 Varo, R., . . . Gutierrez, A. (2018). Phagocytic clearance of presynaptic dystrophies by

reactive astrocytes in Alzheimer's disease. *Glia, 66*(3), 637-653. doi:10.1002/glia.23270

Gomez-Isla, T., Hollister, R., West, H., Mui, S., Growdon, J. H., Petersen, R. C., . . . Hyman, B. T. (1997). Neuronal loss correlates with but exceeds neurofibrillary tangles in Alzheimer's disease. *Ann Neurol, 41*(1), 17-24. doi:10.1002/ana.410410106

Graves, S. M., Xie, Z., Stout, K. A., Zampese, E., Burbulla, L. F., Shih, J. C., . . . Surmeier, D. J. (2020). Dopamine metabolism by a monoamine oxidase mitochondrial shuttle activates the electron transport chain. *Nat Neurosci, 23*(1), 15-20. doi:10.1038/s41593-019-0556-3

Grubman, A., Chew, G., Ouyang, J. F., Sun, G. Z., Choo, X. Y., McLean, C., . . . Polo, J. M. (2019). A single-cell atlas of entorhinal cortex from individuals with Alzheimer's disease reveals cell-type-specific gene expression regulation. *Nature Neuroscience, 22*(12), 2087-+. doi:10.1038/s41593-019-0539-4

Habib, N., McCabe, C., Medina, S., Varshavsky, M., Kitsberg, D., Dvir-Szternfeld, R., . . . Schwartz, M. (2020). Disease-associated astrocytes in Alzheimer's disease and aging. *Nature Neuroscience, 23*(6), 701-706. doi:10.1038/s41593-020-0624-8

Han, Z., Qu, J., Zhao, J., & Zou, X. (2018). Analyzing 74,248 Samples Confirms the Association Between CLU rs11136000 Polymorphism and Alzheimer's Disease in Caucasian But Not Chinese population. *Sci Rep, 8*(1), 11062. doi:10.1038/s41598-018-29450-2

Hanzelmann, S., Castelo, R., & Guinney, J. (2013). GSVA: gene set variation analysis for microarray and RNA-seq data. *BMC Bioinformatics, 14*, 7. doi:10.1186/1471-2105-14-7

Hoffman, J. M., Welsh-Bohmer, K. A., Hanson, M., Crain, B., Hulette, C., Earl, N., & Coleman, R. E. (2000). FDG PET imaging in patients with pathologically verified dementia. *J Nucl Med, 41*(11), 1920-1928.

Iram, T., Trudler, D., Kain, D., Kanner, S., Galron, R., Vassar, R., . . . Frenkel, D. (2016). Astrocytes from old Alzheimer's disease mice are impaired in Abeta uptake and in neuroprotection. *Neurobiol Dis, 96*, 84-94. doi:10.1016/j.nbd.2016.08.001

Jo, S., Yarishkin, O., Hwang, Y. J., Chun, Y. E., Park, M., Woo, D. H., . . . Lee, C. J. (2014). GABA from reactive astrocytes impairs memory in mouse models of Alzheimer's disease. *Nat Med, 20*(8), 886-896. doi:10.1038/nm.3639

Kelley, K. W., Nakao-Inoue, H., Molofsky, A. V., & Oldham, M. C. (2018). Variation among intact tissue samples reveals the core transcriptional features of human CNS cell classes. *Nat Neurosci, 21*(9), 1171-1184. doi:10.1038/s41593-018-0216-z

Kryuchkova-Mostacci, N., & Robinson-Rechavi, M. (2017). A benchmark of gene expression tissue-specificity metrics. *Brief Bioinform, 18*(2), 205-214. doi:10.1093/bib/bbw008

Lee, Y. F., Gerashchenko, D., Timofeev, I., Bacskai, B. J., & Kastanenka, K. V. (2020). Slow Wave Sleep Is a Promising Intervention Target for Alzheimer's Disease. *Frontiers in Neuroscience, 14*(705). doi:10.3389/fnins.2020.00705

Liddelow, S. A., Marsh, S. E., & Stevens, B. (2020). Microglia and Astrocytes in Disease: Dynamic Duo or Partners in Crime? *Trends Immunol, 41*(9), 820-835. doi:10.1016/j.it.2020.07.006

Lin, S. M., Du, P., Huber, W., & Kibbe, W. A. (2008). Model-based variance-stabilizing transformation for Illumina microarray data. *Nucleic Acids Research, 36*(2), e11-e11. doi:10.1093/nar/gkm1075

Marlatt, M. W., Bauer, J., Aronica, E., van Haastert, E. S., Hoozemans, J. J., Joels, M., & Lucassen, P. J. (2014). Proliferation in the Alzheimer hippocampus is due to microglia,

936 not astroglia, and occurs at sites of amyloid deposition. *Neural Plast, 2014*, 693851.
937 doi:10.1155/2014/693851
938 Marsh, J., & Alifragis, P. (2018). Synaptic dysfunction in Alzheimer's disease: the effects of
939 amyloid beta on synaptic vesicle dynamics as a novel target for therapeutic
940 intervention. *Neural Regen Res, 13*(4), 616-623. doi:10.4103/1673-5374.230276
941 Martini-Stoica, H., Cole, A. L., Swartzlander, D. B., Chen, F., Wan, Y. W., Bajaj, L., . . . Zheng,
942 H. (2018). TFEB enhances astroglial uptake of extracellular tau species and reduces
943 tau spreading. *J Exp Med, 215*(9), 2355-2377. doi:10.1084/jem.20172158
944 Masgrau, R., Guaza, C., Ransohoff, R. M., & Galea, E. (2017). Should We Stop Saying 'Glia'
945 and 'Neuroinflammation'? *Trends Mol Med, 23*(6), 486-500.
946 doi:10.1016/j.molmed.2017.04.005
947 Mathys, H., Davila-Velderrain, J., Peng, Z. Y., Gao, F., Mohammadi, S., Young, J. Z., . . . Tsai,
948 L. H. (2019). Single-cell transcriptomic analysis of Alzheimer's disease (vol 570, pg 332,
949 2019). *Nature, 571*(7763), E1-E1. doi:10.1038/s41586-019-1329-6
950 Misra, J. R., & Irvine, K. D. (2018). The Hippo Signaling Network and Its Biological Functions.
951 *Annu Rev Genet, 52*, 65-87. doi:10.1146/annurev-genet-120417-031621
952 Neff, R. A., et al. (2021). Molecular subtyping of Alzheimer's disease using RNA sequencing
953 data reveals novel mechanisms and targets. *Science Advances, 7*.
954 doi:10.1126/sciadv.abb5398
955 Neuropathology Group. Medical Research Council Cognitive, F., & Aging, S. (2001).
956 Pathological correlates of late-onset dementia in a multicentre, community-based
957 population in England and Wales. Neuropathology Group of the Medical Research
958 Council Cognitive Function and Ageing Study (MRC CFAS). *Lancet, 357*(9251), 169-
959 175. doi:10.1016/s0140-6736(00)03589-3
960 Orre, M., Kamphuis, W., Osborn, L. M., Jansen, A. H. P., Kooijman, L., Bossers, K., & Hol, E.
961 M. (2014). Isolation of glia from Alzheimer's mice reveals inflammation and
962 dysfunction. *Neurobiol Aging, 35*(12), 2746-2760.
963 doi:10.1016/j.neurobiolaging.2014.06.004
964 Pelvig, D. P., Pakkenberg, H., Regeur, L., Oster, S., & Pakkenberg, B. (2003). Neocortical glial
965 cell numbers in Alzheimer's disease. A stereological study. *Dement Geriatr Cogn*
966 *Disord, 16*(4), 212-219. doi:10.1159/000072805
967 Perez-Nievas, B. G., & Serrano-Pozo, A. (2018). Deciphering the Astrocyte Reaction in
968 Alzheimer's Disease. *Front Aging Neurosci, 10*, 114. doi:10.3389/fnagi.2018.00114
969 Rodriguez-Vieitez, E., Saint-Aubert, L., Carter, S. F., Almkvist, O., Farid, K., Schöll, M., . . .
970 Nordberg, A. (2016). Diverging longitudinal changes in astrocytosis and amyloid PET
971 in autosomal dominant Alzheimer's disease. *Brain, 139*(Pt 3), 922-936.
972 doi:10.1093/brain/awv404
973 Saddawi-Konefka, R., Seelige, R., Gross, E. T., Levy, E., Searles, S. C., Washington, A., Jr., . . .
974 Bui, J. D. (2016). Nrf2 Induces IL-17D to Mediate Tumor and Virus Surveillance. *Cell*
975 *Rep, 16*(9), 2348-2358. doi:10.1016/j.celrep.2016.07.075
976 Sakers, K., Lake, A. M., Khazanchi, R., Ouwenga, R., Vasek, M. J., Dani, A., & Dougherty, J.
977 D. (2017). Astrocytes locally translate transcripts in their peripheral processes. *Proc*
978 *Natl Acad Sci U S A, 114*(19), E3830-E3838. doi:10.1073/pnas.1617782114
979 Sanchez-Mico, M. V., Jimenez, S., Gomez-Arboledas, A., Munoz-Castro, C., Romero-Molina,
980 C., Navarro, V., . . . Vitorica, J. (2020). Amyloid-beta impairs the phagocytosis of
981 dystrophic synapses by astrocytes in Alzheimer's disease. *Glia*. doi:10.1002/glia.23943

982 Santello, M., Bezzi, P., & Volterra, A. (2011). TNFα controls glutamatergic gliotransmission in
983 the hippocampal dentate gyrus. *Neuron, 69*(5), 988-1001.
984 doi:10.1016/j.neuron.2011.02.003
985 Sekar, S., McDonald, J., Cuyugan, L., Aldrich, J., Kurdoglu, A., Adkins, J., . . . Liang, W. S.
986 (2015). Alzheimer's disease is associated with altered expression of genes involved in
987 immune response and mitochondrial processes in astrocytes. *Neurobiology of Aging,*
988 *36*(2), 583-591. doi:10.1016/j.neurobiolaging.2014.09.027
989 Shi, Q., & Gibson, G. E. (2007). Oxidative stress and transcriptional regulation in Alzheimer
990 disease. *Alzheimer Dis Assoc Disord, 21*(4), 276-291.
991 doi:10.1097/WAD.0b013e31815721c3
992 Simpson, J. E., Ince, P. G., Shaw, P. J., Heath, P. R., Raman, R., Garwood, C. J., . . . Ne, M. C.
993 F. A. (2011). Microarray analysis of the astrocyte transcriptome in the aging brain:
994 relationship to Alzheimer's pathology and APOE genotype. *Neurobiology of Aging,*
995 *32*(10), 1795-1807. doi:10.1016/j.neurobiolaging.2011.04.013
996 Sollvander, S., Nikitidou, E., Brolin, R., Soderberg, L., Sehlin, D., Lannfelt, L., & Erlandsson,
997 A. (2016). Accumulation of amyloid-beta by astrocytes result in enlarged endosomes
998 and microvesicle-induced apoptosis of neurons. *Mol Neurodegener, 11*(1), 38.
999 doi:10.1186/s13024-016-0098-z
1000 Swerdlow, R. H. (2018). Mitochondria and Mitochondrial Cascades in Alzheimer's Disease.
1001 *Journal of Alzheimers Disease, 62*(3), 1403-1416. doi:10.3233/Jad-170585
1002 Torper, O., & Gotz, M. (2017). Brain repair from intrinsic cell sources: Turning reactive glia
1003 into neurons. *Functional Neural Transplantation Iv: Translation to Clinical*
1004 *Application, Pt A, 230*, 69-97. doi:10.1016/bs.pbr.2016.12.010
1005 Weirauch, M. (2011). *Gene Coexpression Networks for the Analysis of DNA Microarray Data*
1006 (P. D. M. D. P. D. F. E. S. A. G. A. Salvador Ed. Vol. 1). Applied Statistics for Network
1007 Biology: Methods in Systems Biology, Volume 1.
1008 Wyss-Coray, T., Loike, J. D., Brionne, T. C., Lu, E., Anankov, R., Yan, F., . . . Husemann, J.
1009 (2003). Adult mouse astrocytes degrade amyloid-β in vitro and in situ. *Nature*
1010 *Medicine, 9*(4), 453-457. doi:10.1038/nm838
1011 Xie, C., Shen, X., Xu, X., Liu, H., Li, F., Lu, S., . . . Huang, Z. (2020). Astrocytic YAP Promotes
1012 the Formation of Glia Scars and Neural Regeneration after Spinal Cord Injury. *J*
1013 *Neurosci, 40*(13), 2644-2662. doi:10.1523/JNEUROSCI.2229-19.2020
1014 Zhang, B., Gaiteri, C., Bodea, L. G., Wang, Z., McElwee, J., Podtelezhnikov, A. A., . . . Emilsson,
1015 V. (2013). Integrated systems approach identifies genetic nodes and networks in late-
1016 onset Alzheimer's disease. *Cell, 153*(3), 707-720. doi:10.1016/j.cell.2013.03.030
1017 Zhang, Y., Sloan, S. A., Clarke, L. E., Caneda, C., Plaza, C. A., Blumenthal, P. D., . . . Barres, B.
1018 A. (2016). Purification and Characterization of Progenitor and Mature Human
1019 Astrocytes Reveals Transcriptional and Functional Differences with Mouse. *Neuron,*
1020 *89*(1), 37-53. doi:10.1016/j.neuron.2015.11.013

1021

1022

1023

1024 # Main figures

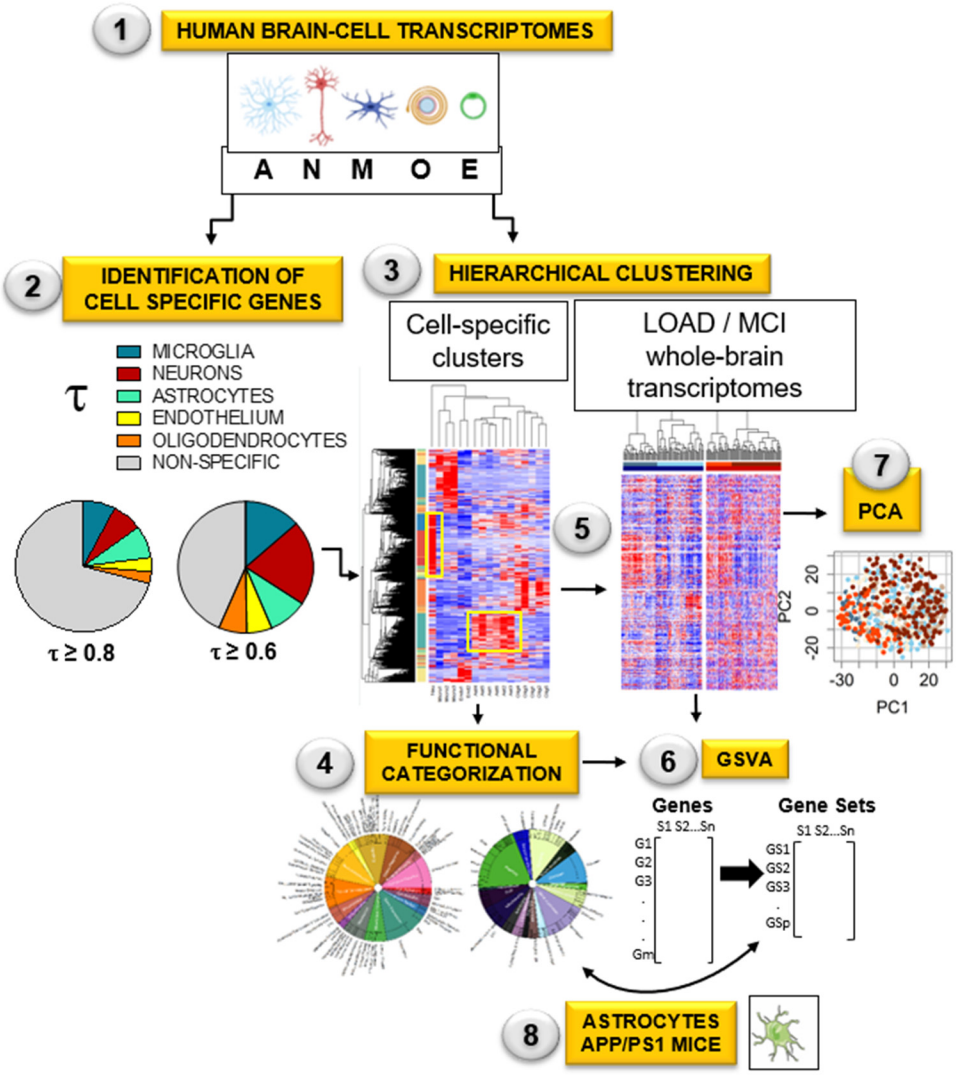

1025

1026 **Figure 1. Workflow for the identification of altered astrocytic functions in AD and MCI**
1027 (See Methods for details).
1028 *Step1*: Genes from human databases were prepared to be classified as cell-specific or enriched using
1029 RNAseq data from cells isolated from aged healthy human brains using the univariate cell-type
1030 enrichment τ scoring (*Step 2*) and hierarchical clustering (*Step 3*). *Step 4*: The astrocytic and neuronal
1031 gene clusters were manually categorized. *Step 5*: The clusters were localized in control, AD and MCI
1032 whole-brain transcriptomes from the MtSINAI, MAYO and ROSMAP databases. *Step 6*: Alterations
1033 of astrocytic and neuronal functional categories in AD and MCI groups versus controls was statistically
1034 established using (*Step 6*) gene set variation analysis (GSVA), and (*Step 7*) principal component
1035 analysis (PCA). *Step 8*: To compare patients with mice, the published transcriptome of APP/PS1
1036 astrocytes was re-analyzed using GSVA and our functional categorization and GSVA. The figure in
1037 Step 1 was created using cell art adapted from Servier Medical Art (https://smart.servier.com/).

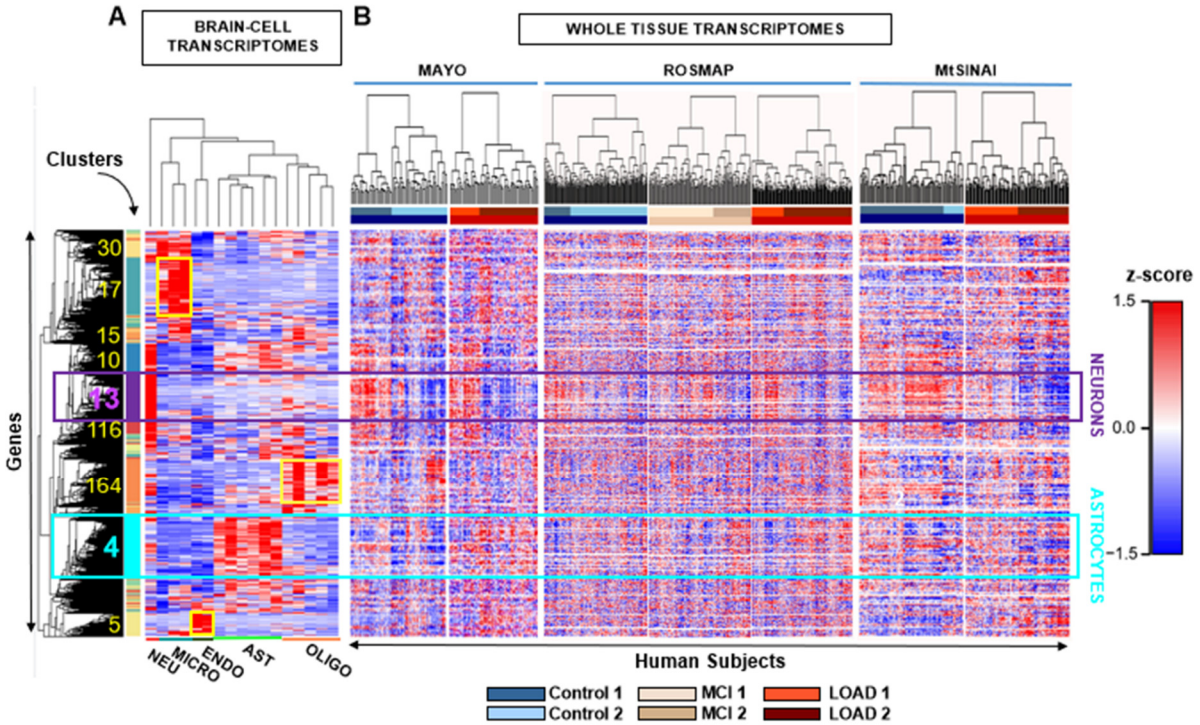

Figure 2. Identification of cell-specific gene clusters in whole-brain transcriptomes by two-step hierarchical clustering.

A. Hierarchical clustering was performed on transcriptomes of brain cell populations isolated from individual healthy subjects. Each column is a sample from a single subject/patient and each row is a z-scored gene. In yellow, the number and location of clusters with highest z scores, coinciding with highest τ scores for a given cell type (cluster information in **Supplementary file 1**, tabs 6-8). The turquoise and purple squares are the main astrocytic and neuronal clusters (cluster # 4 and cluster # 13), respectively. Microglia, oligodendrocyte and endothelial-cell clusters are 17, 164 and 5, respectively (shown in yellow). Clusters 30, 15, 10 and 116 are highly enriched in microglial or neuronal genes, but fall below the criteria established for cell-specificity (**Methods**).

B. Whole-brain transcriptomes from individual subjects of control (blue), MCI (beige) and AD (red) groups from MAYO, ROSMAP, MtSINAI were hierarchically clustered. The rows from the cell-type clustering in **A.** were kept fixed to identify cell-specific clusters. The figure was generated with raw data before correction for cell composition. Clustering of subjects segregated all cohorts into at least 2 subgroups (defined as 1 and 2) showing opposite changes in gene-expression.

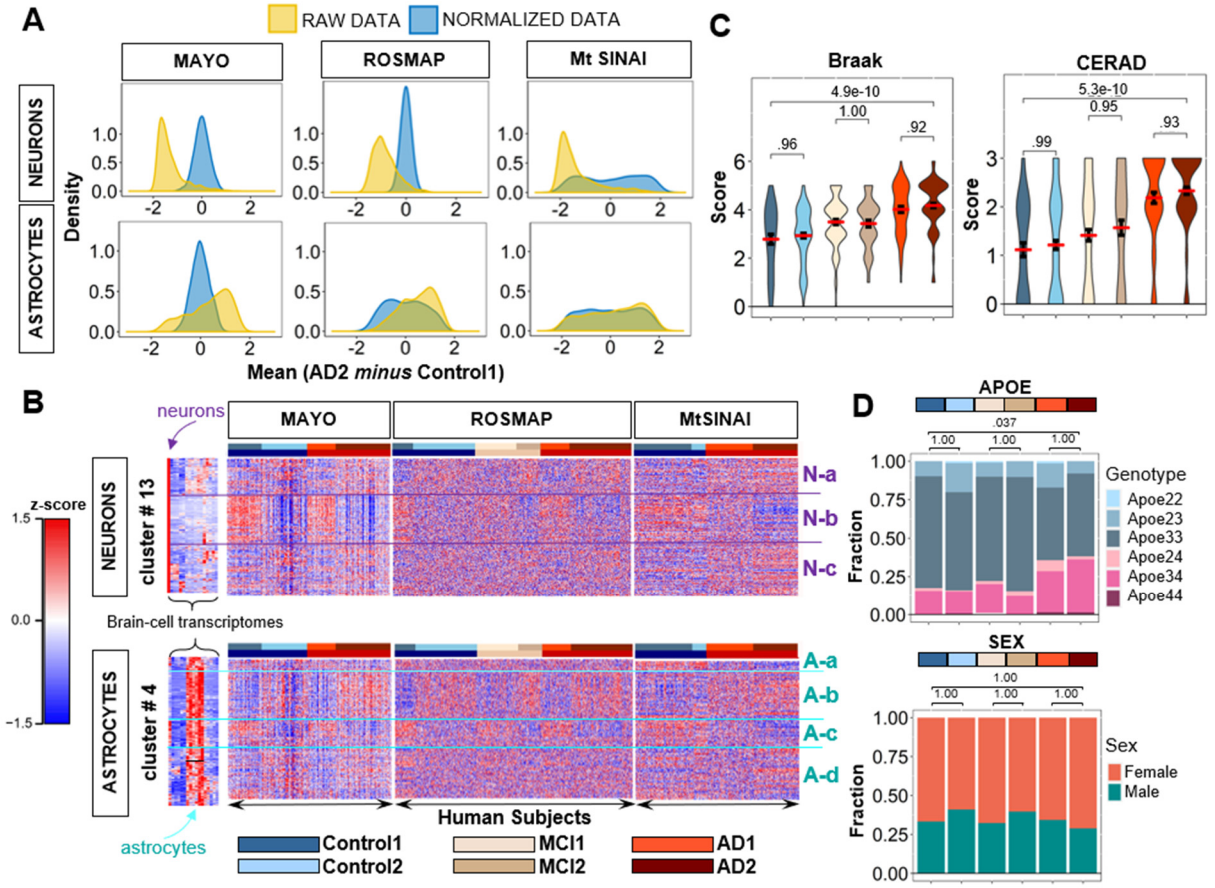

Figure 3. Neuronal and astrocytic gene sub-clusters in the three clinical databases.

A. Distributions of gene expression differences between AD2 and Control1 cohorts before (yellow) and after (blue) variance stabilizing normalization, yielding zero-centered distributions (**Methods**).

B. Hierarchical clustering of Control (blue), MCI (beige), and AD (red) subjects from Fig. 2B using normalized data from Fig. 3A in rows. For both astrocytic and neuronal genes, subjects self-organized into at least two distinct subgroups (defined as 1 and 2) within each clinical group, while genes self-organized into up to four groups (Na-c and Aa-d). In MAYO and ROSMAP, clusters showed opposite directions of change in *type 1* and *2* subjects. In MtSINAI, Control2 was like Control1, and AD1 like AD2, although with less pronounced changes.

C. Violin plots of pathological stages according to CERAD and Braak scoring shows no significant difference in pathological stages between sub-groups within each cohort in ROSMAP (means ± SEM, one-way ANOVA with Tukey post-hoc).

D. Distribution of *APOE* genotypes and sex in the six groups. While 3/3 was the predominant genotype across all groups, and 3/4 was more abundant in AD, there were no differences in frequency of *APOE4* alleles between *type 1* and *2* subgroups within each clinical group. Likewise, females were more abundant than males in all groups, but not in *type 2* subjects as compared to *type 1* (p values determined by pairwise Fisher's Exact test with Bonferroni adjustment).

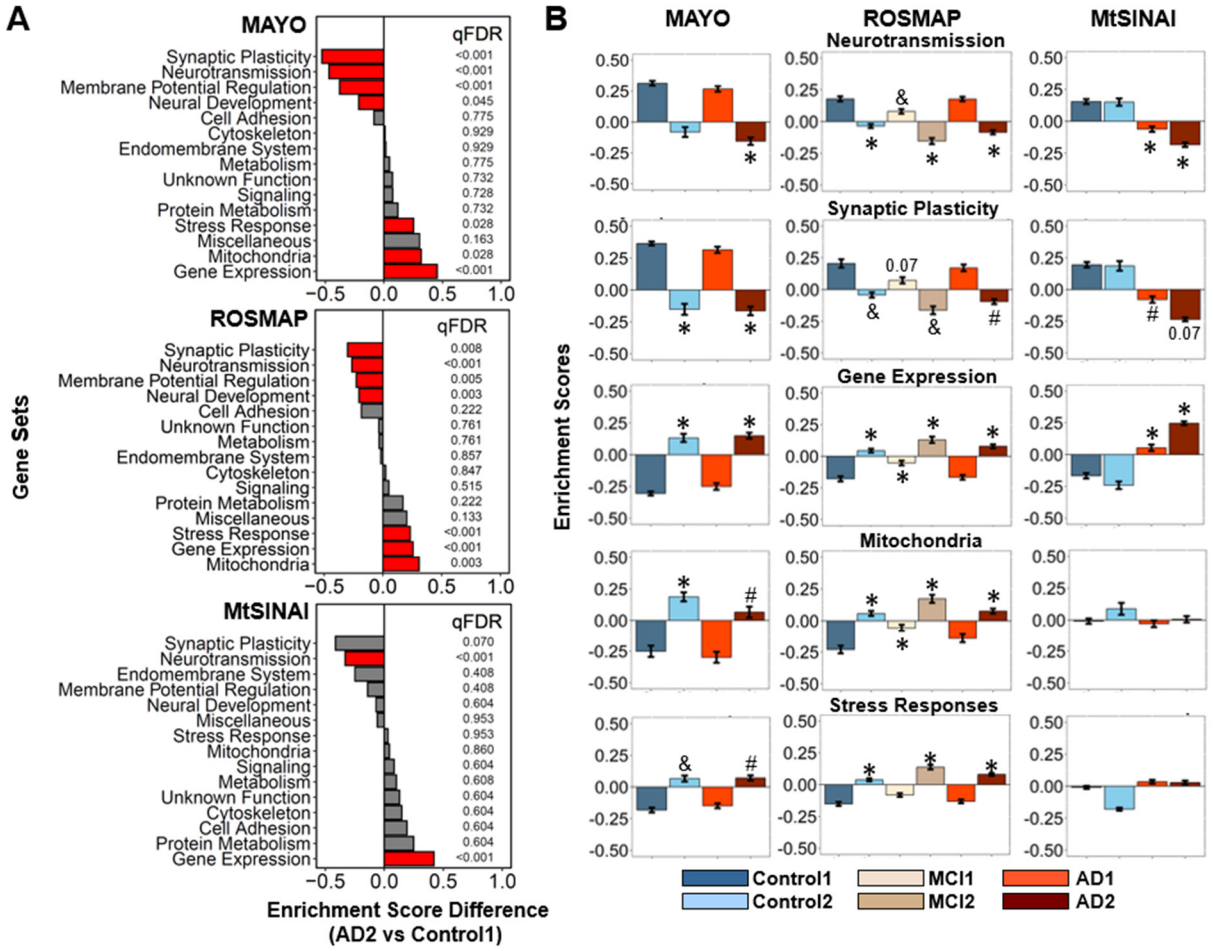

Figure 4. GSVA unravels neuron-enriched functions altered in AD. Differences in the general functional categories among cohorts in MAYO, ROSMAP and MtSINAI databases were examined by GSVA.

A. Comparison between AD2 and Control1. Functions are ranked according to the difference in enrichment scores (ES). Significantly changed functions (qFDR < 0.05) are labeled in red.

B. Enrichment scores of functional categories significantly changed in at least 2 out of 3 databases. (#) qFDR< 0.05 (&) qFDR <0.01, and (*) qFDR < 0.001, versus Control1.

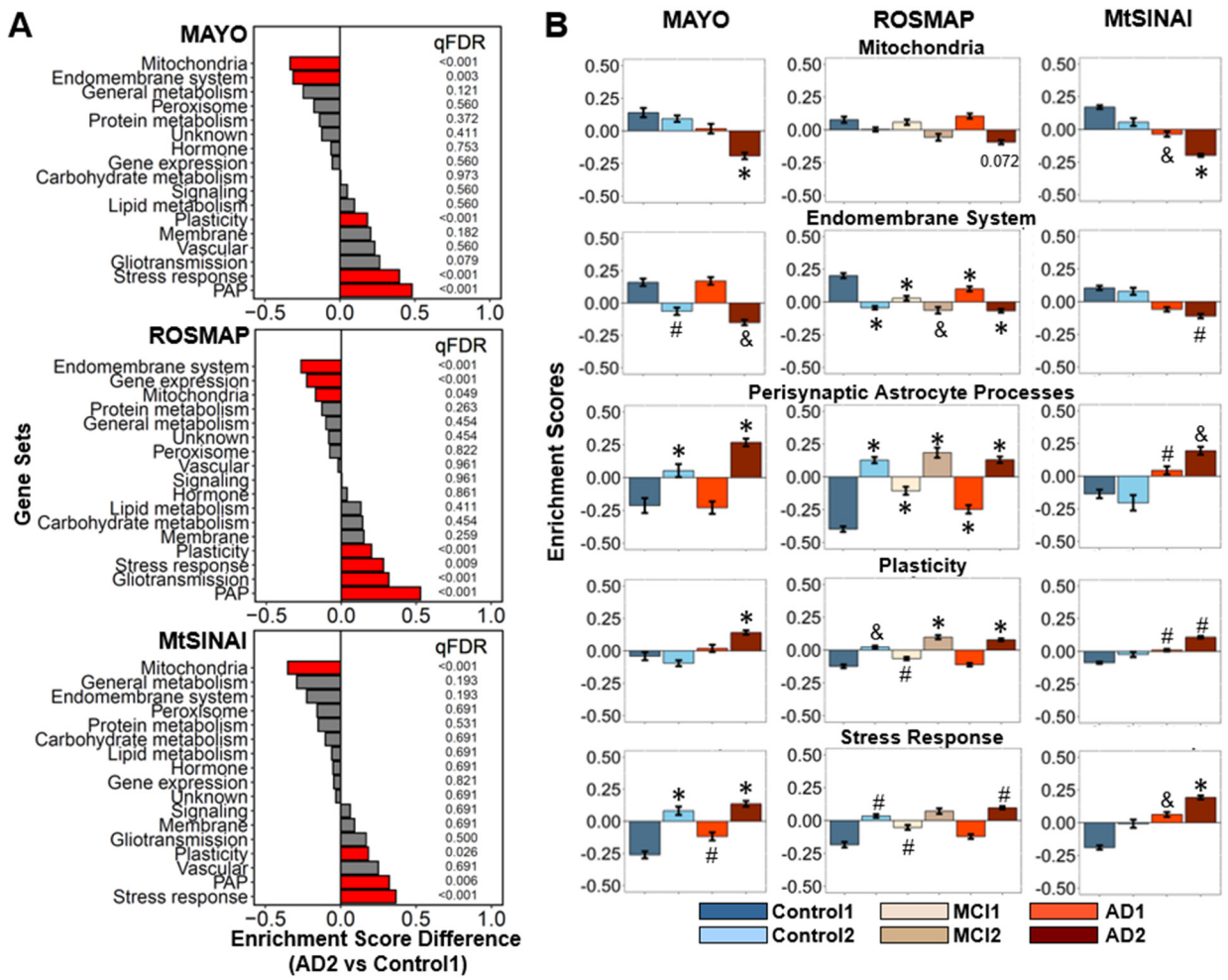

Figure 5. **GSVA unravels astrocyte-enriched functions altered in AD.** Differences in the functional categories among cohorts in MAYO, ROSMAP and MtSINAI databases were examined by GSVA.

A. Comparison between AD2 and Control1. Functions are ranked according to the difference in enrichment scores (ES). Significantly changed functions (qFDR < 0.05) are labeled in red.

B. Enrichment scores of functional categories significantly changed in at least 2 out of 3 databases. (#) qFDR < 0.05, (&) qFDR <0.01, and (*) qFDR < 0.001, versus Control1.

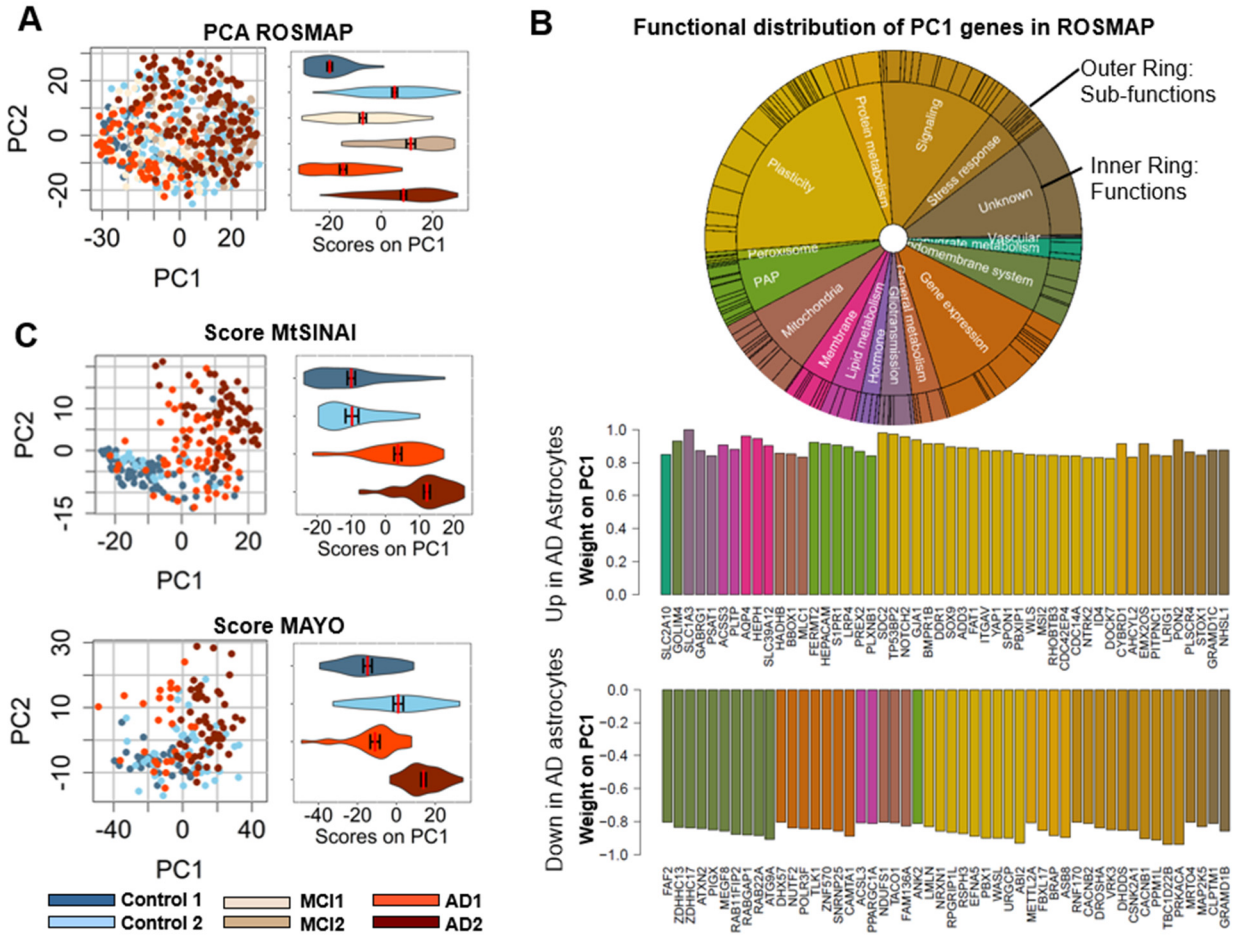

Figure 6. PCA identifies top altered functions in AD astrocytes.

A. PCA analysis of astrocyte-enriched genes in ROSMAP. Dot plots and violin plots along PC1 (mean ± SEM) show differential expression of astrocyte genes in type 2 versus *type 1* subjects.

B. Top varying genes in PC1 (up-regulated and down-regulated), color-coded for function according to the circos plot, inform about functions altered in AD astrocytes. The vertical axis represents the relative contribution (importance/weight) of each gene for the scoring of individual samples in panel **A** along PC1.

C. Scoring of MtSINAI and MAYO databases using genes overlapping with ROSMAP PCA in **A.** discriminates Control and AD cohorts along PC1, as shown by the dot and violin plots (means ± SEM).

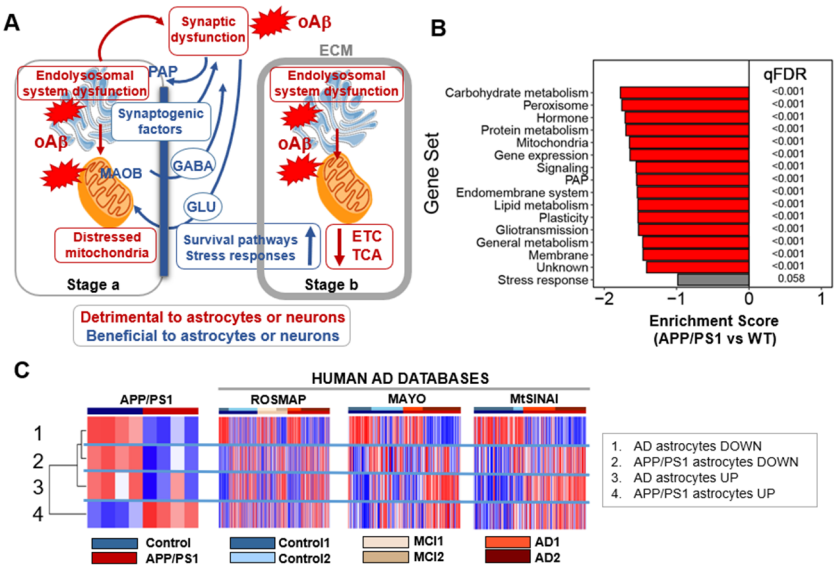

Figure 7. Model of cortical human AD astrocytes and comparison with mice. A. The model revolves around two predictions.

First prediction: amyloid-β drives the phenotypical change of cortical astrocytes in AD by direct and indirect mechanisms. Direct: Amyloid-β causes endolysosomal and mitochondrial dysfunction in astrocytes, resulting in an adaptive astroprotective shift of gliotransmission to a GABA-predominant mode as a strategy to preserve mitochondrial respiration. Indirect: Synaptic dysfunction caused by amyloid-β in neurons augments the production of the PAP machinery and synaptogenic factors in astrocytes—a phenomenon of enhanced astrocytic plasticity to protect neurons.

Second prediction: the phenotypical transformation of astrocytes in AD happens in early and late stages. Control2 subjects, cognitively normal, would be at stage a, and AD2 patients, diagnosed with dementia, at stage b. In stage a, the astroprotective change in glutamate/GABA fluxes may preserve neural-circuit homeostasis, because the GABA produced by MAO-B may locally compensate for the deficits in inhibitory tone that disrupts circuitry synchronization (Lee et al., 2020). By contrast, deficits in the endolysosomal system would result in partial phagocytosis of amyloid-β (Sollvander et al., 2016) and dystrophic neurites (Gomez-Arboledas et al., 2018), thus exacerbating amyloid-β accumulation, and hindering neuronal repair due to lack of debris elimination. In stage b, the mechanisms triggered to protect mitochondria may fail, and cortical astrocytes become deeply malfunctional, as suggested by the reduction in TCA cycle and ETC transcripts, despite the increase in protective stress responses and pro-survival pathways aimed at preventing astrocyte demise. For simplicity, only predominantly altered functions are depicted. ECM, extracellular matrix; ETC: electron transport chain, GLU: glutamate; oAβ: oligomeric amyloid-β; PAP: perisynaptic astrocyte processes; TCA: tricarboxylic acid. Figure adapted from Servier Medical Art (https://smart.servier.com/).

1123 **B**. GSVA of the transcriptome of astrocytes isolated from APP/PS1 mouse cortices using our manually
1124 curated functional categorization shows downregulation of astrocyte-enriched functions.
1125 **C.** Left, GSVA of transcriptome of APP/PS1 astrocytes according to the top dysregulated astrocyte
1126 genes in PC1 from the ROSMAP database (**Fig. 6B**). Astrocyte-enriched genes dysregulated in AD (up
1127 and down) are down-regulated in APP/PS1 astrocytes, as shown in B. Right, GSVA of PC1 AD and
1128 mouse APP/PS1 DEG gene sets in ROSMAP, MAYO and MtSINAI whole-brain transcriptomes shows
1129 that both the up and down-regulated mouse genes pools tend to be up-regulated in AD databases.
1130
1131
1132
1133

Supplementary files

1134 **Supplementary file 1**. **Generation of cell-specific gene modules.** Tabs:
1135 1. Tab description.
1136 2. Transcriptomic databases of human-brain cells obtained from (Y. Zhang et al., 2016).
1137 3. PCA of transcriptomic data of astrocytes isolated from young (<47 years old) and old (>47 years
1138 old) shows that they were significantly different.
1139 4. Specific data used for τ scoring and hierarchical clustering.
1140 5. Top τ scores per gene, indicating which cell type presents that score; and pie charts of the
1141 distribution of specific and enriched genes among brain cells.
1142 6. Raw results of hierarchical clustering.
1143 7. Cluster description.
1144 8. Cluster selection.

1145 **Supplementary file 2. Functional categories of astrocytic and neuronal modules.** Tabs:
1146 1. Circo plots showing functional categories (inner ring) and subcategories (outer ring) of
1147 astrocytic gene cluster 4 (1650 genes) and neuronal gene cluster 13 (1258 genes). For astrocytes,
1148 there are 17 groups and 133 subgroups. For neurons, 15 groups and 76 subgroups.
1149 2. Functional categorization of neuronal cluster 13.
1150 3. Functional categorization of astrocytic cluster 4.

1151 **Supplementary file 3. Hierarchical clustering of astrocytic and neuronal gene sets**
1152 **before and after data normalization.** Gene expressions were normalized according to the
1153 probabilistic distribution of relative expressions to reach distribution peaks of zero (Methods).
1154 Normalization improved the resolution of astrocytic and neuronal gene clusters between and within
1155 cohorts.
1156

1157 **Supplementary file 4.** Cluster # 4 expression in the three databases after data normalization. The

1158 statistical comparison between AD2 and Control1 was performed by the Wilcoxon rank sum test.
1159 Statistical significance pFDR < 0.05. Consensus dysregulated genes are indicated in color: blue, down-
1160 regulated; yellow, up-regulated, and grey, unchanged.
1161
1162 **Supplementary file 5.** GSVA statistics of inter-cohort comparisons of changes in neuronal and
1163 astrocytic *general* functions in MAYO, ROSMAP and MtSINAI databases. Comparisons: ROSMAP:
1164 Control2 vs Control1 (pFDR1), MCI1 vs Control1 (pFDR2), MCI2 vs Control1 (pFDR3), AD1 vs
1165 Control1 (pFDR4), AD2 vs Control1 (pFDR4). MAYO and MtSINAI: Control2 vs Control1
1166 (pBootFDR1), AD1 vs Control1 (pFDR2), AD2 vs Control1 (pFDR3). Tabs:
1167 1. Functional categories in neurons.
1168 2. Functional categories in astrocytes.
1169
1170 **Supplementary file 6. Extended Fig. 4B. Alteration of neuron-enriched functions in AD.**
1171 Enrichment scores of functional categories significantly changed in at least 2 out of 3 databases. (&)
1172 pFDR <0.01, (#) pFDR < 0.05 and (*) pFDR < 0.001, versus Control1.
1173
1174 **Supplementary file 7. Correlations between changes in neuronal general functional**
1175 **categories and pathological stages**. Bolded numbers are probability of a zero slope for linear
1176 model.
1177 A. Braak scores.
1178 B. CERAD scores.
1179
1180 **Supplementary file 8. Correlations between changes in astrocytic general functional**
1181 **categories and pathological stages.** Bolded numbers are probability of a zero slope for linear
1182 model.
1183 A. Braak scores.
1184 B. CERAD scores.
1185
1186 **Supplementary file 9. Correlations among altered functions in the ROSMAP, MAYO,**
1187 **and MtSINAI databases.**
1188 **A**, **C**, **E**. Hierarchical clustering of Pearson correlation coefficients. The enrichment scores of all
1189 functions across all samples were correlated with one another (Methods). Clustering segregated
1190 correlations in two main branches that grouped down-regulated (branch 1) and up-regulated
1191 functions (branch 2), respectively. Functions found altered in at least two out of the three databases
1192 are labeled in blue (down-regulated) or red (up-regulated) squares. Strongest direct correlations were
1193 among highly related biological processes such as 'membrane potential', 'neurotransmission' and
1194 'synaptic plasticity' in neurons, and 'PAP' and 'gliotransmission' in astrocytes (orange scale). The

1195 strongest anti-correlations (i.e., concomitant changes in opposite directions, grey scale) were: (i)
1196 down-regulation of synaptic functions versus up-regulation of neuronal 'mitochondria', 'stress
1197 response' and 'gene expression' (dark green squares); (ii) decrease in synaptic functions versus up-
1198 regulation of 'PAP/gliotransmission' and 'plasticity' in astrocytes (light green squares); (iii) in
1199 astrocytes, increases in 'PAP/gliotransmission' versus down-regulation of 'endomembrane system'
1200 and 'gene expression', and 'plasticity' versus 'mitochondria' (pink squares). In summary, anti-
1201 correlations (negative p-values) point to highly intertwined changes between morphological
1202 remodeling in astrocytes and neuronal dysfunction, and between survival responses and organelle
1203 dysfunctions in astrocytes.
1204 **B**, **D**, **F**. Heatmap of FDR adjusted p-values. In red, adj FDR p-values < 0.05

1205 **Supplementary file 10.** GSVA statistics of inter-cohort comparisons of changes in neuronal and
1206 astrocytic *subcategories* in MAYO, ROSMAP and MtSINAI databases. Comparisons: Control2 vs
1207 Control1 (pFDR1), AD1 vs Control1 (pFDR2), AD2 vs Control1 (pFDR3). Tabs:
1208 1. All functional subcategories/MAYO.
1209 2. All functional subcategories /ROSMAP.
1210 3. All functional subcategories /MtSINAI.
1211 4. PAP / all databases.
1212 5. Gliotransmission / all databases.
1213 6. Plasticity /all databases.
1214 7. Stress response /all databases.
1215 8. Mitochondria in all data /all databases.
1216 9. Endolysosomal system /all databases.

1217 **Supplementary file 11.** Astrocyte cluster # 4 ranked according to PC1 in ROSMAP, and comparison
1218 with DEG identified by snRNAseq in human AD astrocytes (Mathys et al., 2019) (Grubman et al.,
1219 2019). Tabs:
1220 **1.** Venn diagrams.
1221 **2.** Comparison of PC1/ROSMAP with (Mathys et al., 2019).
1222 **3.** Comparison of PC1/ROSMAP with (Grubman et al., 2019).
1223 **4.** Comparison of PC1/ROSMAP between (Mathys et al., 2019) and (Grubman et al., 2019).

1224 **Supplementary file 12.** Comparison of the functional category of cluster # 4 of human astrocytes
1225 containing immunity-related genes with the immunity-related GO groups found significantly
1226 dysregulated in APP/PS1 mouse astrocytes (Orre et al., 2014). Only C1S (Complement Component 1,
1227 S Subcomponent) appears in both gene sets.

1228